The EMBO Journal (2013) 32, 1745–1760
www.embojournal.org

TRANSPARENT PROCESS

THE EMBO JOURNAL

Attenuation of insulin signalling contributes to FSN-1-mediated regulation of synapse development

Wesley L Hung[1], Christine Hwang[1,2], ShangBang Gao[1], Edward H Liao[1,3,5], Jyothsna Chitturi[1,2], Ying Wang[1], Hang Li[1], Christian Stigloher[4,6], Jean-Louis Bessereau[4] and Mei Zhen[1,2,3,*]

[1]Samuel Lunenfeld Research Institute, Mount Sinai Hospital, Toronto, Ontario, Canada, [2]Institute of Medical Science, University of Toronto, Toronto, Ontario, Canada, [3]Department of Molecular Genetics, University of Toronto, Toronto, Ontario, Canada and [4]Institut de Biologie de l'École Normale Supérieure, Biology Department, INSERM, Paris, France

A neuronal F-box protein FSN-1 regulates *Caenorhabditis elegans* neuromuscular junction development by negatively regulating DLK-mediated MAPK signalling. In the present study, we show that attenuation of insulin/IGF signalling also contributes to FSN-1-dependent synaptic development and function. The aberrant synapse morphology and synaptic transmission in *fsn-1* mutants are partially and specifically rescued by reducing insulin/IGF-signalling activity in postsynaptic muscles, as well as by reducing the activity of EGL-3, a prohormone convertase that processes agonistic insulin/IGF ligands INS-4 and INS-6, in neurons. FSN-1 interacts with, and potentiates the ubiquitination of EGL-3 *in vitro*, and reduces the EGL-3 level *in vivo*. We propose that FSN-1 may negatively regulate insulin/IGF signalling, in part, through EGL-3-dependent insulin-like ligand processing.

The EMBO Journal (2013) **32,** 1745–1760. doi:10.1038/emboj.2013.91; Published online 10 May 2013
Subject Categories: signal transduction; neuroscience
Keywords: *fsn-1* ubiquitin ligase; insulin/IGF signalling; synapse development

Introduction

In both invertebrate and vertebrate nervous systems, insulin signalling has been implicated in synapse development, function and plasticity. Insulin stimulates the clustering of neurotransmitter receptors in mammalian neuron cultures (Man *et al*, 2000; Mielke and Wang, 2005), and potently inhibits the firing of specific groups of hypothalamus neurons (Plum *et al*, 2006; Klockener *et al*, 2011). In *C. elegans*, insulin/IGF signalling has been implicated in chemotaxis (Tomioka *et al*, 2006), thermotaxis (Murakami *et al*, 2005) and learning (Lin *et al*, 2010; Chen *et al*, 2012). Reducing insulin signalling in the retinotectal neurons of *Xenopus* tadpoles leads to a drastic decrease in the number of glutamatergic synapses and a reduced response to light stimuli (Chiu *et al*, 2008). Impaired insulin and IGF-signalling-mediated synaptic dysfunction has been further implicated in neurological disorders, including Alzheimer's disease (Gault and Holscher, 2008; De Felice *et al*, 2009; Lee *et al*, 2009) and Rett Syndrome (Liao and Xu, 2009; Tong *et al*, 2009; Tropea *et al*, 2009). In *C. elegans*, insulin/IGF signalling also affects neuronal aging (Pan *et al*, 2011; Tank *et al*, 2011; Toth *et al*, 2012). However, how insulin/IGF-signalling activity is regulated to affect the nervous system development and function remains unknown.

Molecular components of the *C. elegans* and mammalian insulin/IGF-signalling pathways exhibit a remarkable degree of conservation (reviewed in Mukhopadhyay *et al*, 2006; Kleeman and Murphy, 2009; Kaletsky and Murphy, 2010; Kenyon, 2010). The canonical insulin/IGF-signalling cascade in *C. elegans*, essential for viability, involves a single insulin/IGF-like receptor tyrosine kinase (InR) DAF-2 (Kenyon *et al*, 1993; Kimura *et al*, 1997), and the sequential activation of the phosphoinositide-3 (PI-3) kinase AGE-1 (Morris *et al*, 1996), the PI-3-dependent kinase PDK-1, and two serine/threonine kinases AKT-1 and AKT-2 (Paradis and Ruvkun, 1998; Paradis *et al*, 1999). One of the main downstream effectors of insulin/IGF signalling is the Forkhead (FOXO) transcription factor DAF-16 (Ogg *et al*, 1997; Lee *et al*, 2001; Lin *et al*, 2001). Activation of insulin/IGF signalling results in the phosphorylation of DAF-16, preventing its translocation to the nucleus and inhibiting its activity as a transcriptional regulator in diverse biological processes including the activation of alternative development programme, metabolism, longevity, immunity, stress response and aging (Riddle *et al*, 1981; Kenyon *et al*, 1993; Lee *et al*, 2003; Berdichevsky *et al*, 2006; Landis and Murphy, 2010; Pan *et al*, 2011; Tank *et al*, 2011; Chen *et al*, 2012; Toth *et al*, 2012).

The *C. elegans* genome encodes 40 insulin/insulin-like secreted peptides (Pierce *et al*, 2001; Li *et al*, 2003, www.wormbase.org). They are the putative DAF-2/InR ligands to regulate processes described above. Specifically, they may function as either DAF-2/InR agonists or antagonists (Pierce *et al*, 2001; Li *et al*, 2003) to regulate dauer formation, an alternative developmental programme activated under unfavourable environmental conditions (Riddle *et al*, 1981; Golden and Riddle, 1982; Pierce *et al*, 2001). The maturation of mammalian insulin involves sequential processing of a precursor by multiple prohormone convertases (PCs) (Orci *et al*, 1987; Malide *et al*, 1995). The processing events and responsible enzymes that lead to the maturation of *C. elegans* insulin/IGF ligands, however, remain unknown.

*Corresponding author. Department of Molecular Genetics, University of Toronto, Room 870, 600 University Avenue, Toronto, Ontario, Canada M5G 1X5. Tel.: +1 416 586 1592; Fax: +1 416 586 8588;
E-mail: zhen@lunenfeld.ca
[5]Present address: Department of Physiology, McGill University, Montreal, QC, Canada H3G1Y6.
[6]Present address: University of Würzburg, Biocenter/Theodor-Boveri-Institute, Electron Microscopy, Am Hubland, Würzburg 97074, Germany.

Received: 7 October 2012; accepted: 27 March 2013; published online: 10 May 2013

Previously, we identified an F-box protein, FSN-1, as a partner of the *C. elegans* PHR protein RPM-1 to regulate neuromuscular junction (NMJ) development (Liao *et al*, 2004). FSN-1 and RPM-1 are components of an evolutionarily conserved E3 ubiquitin ligase complex that regulates neurite outgrowth and synapse development (Liao *et al*, 2004; Wu *et al*, 2007; Saiga *et al*, 2009; Po *et al*, 2010). *fsn-1* and *rpm-1* mutants share similar synapse morphology defects, where GABAergic NMJs exhibit both over- and under-growth. Loss-of-function mutants for the *Drosophila* orthologs of RPM-1 and FSN-1, *Hiw* and *DFsn*, respectively, exhibit similar synaptic overgrowth and synaptic transmission defects at glutamatergic NMJs (Wu *et al*, 2007). Similarly, knockout mice for the vertebrate homologue of FSN-1/DFsn, Fbxo45, exhibit phenotypes reminiscent of the *Phr1*$^{-/-}$ mice, including respiratory failure at birth and a reduction of axon tracks in the CNS (Burgess *et al*, 2004; Bloom *et al*, 2007; Lewcock *et al*, 2007; Saiga *et al*, 2009).

Several signalling pathways exhibit genetic or biochemical interactions with the PHR and Fbxo45 E3 ligases (reviewed in Po *et al*, 2010). Among them, the MAPKKK kinase DLK-1/Wallenda is a conserved target of the PHR-mediated ubiquitination and degradation. *C. elegans* DLK-1 and the downstream p38 MAPK signalling is negatively regulated by RPM-1 during synapse development (Nakata *et al*, 2005). In *Drosophila,* Wallenda, and its effector JNK/Basket, was identified as genetic suppressor of both *Hiw* and *Dfsn* (Collins *et al*, 2006). Consistent with these findings, *fsn-1* defects are suppressed by mutations in the p38 MAPK pathway, similar to *rpm-1* mutants (this study). p38 MAPK activity is also elevated in the developing growth cones of *Phr*$^{-/-}$- embryonic motor neuron cultures (Lewcock *et al*, 2007).

MAPK mutants exert a robust, but incomplete rescue of the phenotypes of *rpm-1* and *Hiw* mutants (Nakata *et al*, 2005; Collins *et al*, 2006). The levels of DLK family kinases do not exhibit obvious changes in *Phr*$^{-/-}$ or *Fbxo45*$^{-/-}$ mouse mutants (Saiga *et al*, 2009), implying the presence of additional targets for these E3 ligases. In this regard, human PHR/PAM ubiquitinates TSC2 and negatively regulates mTOR signalling in cultured neurons (Murthy *et al*, 2004; Han *et al*, 2008). Similarly, the functional loss of the zebrafish PHR, Esrom, leads to defective commissural axon outgrowth that coincides with an increased mTOR signalling (Hendricks *et al*, 2008).

Here, we report that at *C. elegans* NMJs, attenuation of insulin/IGF signalling also contributes to FSN-1-mediated synaptic development and function. We show that *fsn-1* mutants exhibit defective synaptic morphology and transmission at NMJs, and both defects were robustly, although not fully, rescued by reducing the insulin/IGF-signalling activity. The effect is specific because reducing the insulin/IGF-signalling activity did not lead to significant suppression of *rpm*-1. We further demonstrate that EGL-3 is a *C. elegans* PC that processes multiple neuronal insulin/IGF ligands, and is a component of the insulin-signalling pathway that modifies the *fsn-1* synaptic defects. FSN-1 can physically interact with EGL-3, leading to EGL-3 ubiquitination *in vitro*. FSN-1 also reduces EGL-3 level *in vivo*. We propose that in addition to MAPK signalling, FSN-1 may also affect NMJ development, in part, through attenuation of insulin/IGF signalling.

Results

fsn-1 mutants exhibit aberrant NMJ development

C. elegans motor neurons form *en passant* cholinergic and GABAergic NMJs. Using a fluorescent marker for GABAergic synapses, we previously identified a neuronal F-box protein FSN-1 that regulates the morphology of NMJs (Liao *et al*, 2004). GABAergic NMJs were visualized *in vivo* by either pre- or postsynaptic markers, *juIs1* (*Punc*-25-SNB-1::GFP) and *oxIs22* ($GABA_R$::GFP), respectively, as evenly spaced and discrete fluorescent puncta along the nerve processes (Figure 1B, Supplementary Figure S1A). In *fsn-1* null alleles, both pre- (SNB-1::GFP, Figure 1C) and postsynaptic ($GABA_R$::GFP, Supplementary Figure S1A) markers for GABAergic NMJs exhibited a similar aberrant clustering of fluorescent puncta, accompanied by extended regions devoid of fluorescent signals. These changes resulted in a 43% decrease of the GABAergic NMJ number in *fsn-1* mutants (Figure 1H), while remaining GABAergic NMJs exhibited a broader size distribution (Supplementary Figure S2D).

Morphological changes exhibited by these synaptic markers reflect a general NMJ morphology abnormality in *fsn-1* mutants. Immunofluorescent staining for endogenous GABA receptors (UNC-49) revealed a similar alteration in the NMJ morphology in *fsn-1* animals. Unlike wild-type GABAergic NMJs, where the apposing pre- (SNB-1::GFP) and postsynaptic ($GABA_R$/UNC-49) termini appeared round and even-sized, in *fsn-1* animals, $GABA_R$/UNC-49 signals became unevenly distributed, with large clusters associating with aberrantly clustered presynaptic SNB-1::GFP signals (Supplementary Figure S1A). Similarly, the morphology of cholinergic NMJs, examined by co-immunofluorescent staining of endogenous pre- (VAChT/UNC-17) and postsynaptic (ACh_R/UNC-38) proteins, also exhibited correlated, uneven distribution when compared to that of wild-type animals (Supplementary Figure S1B).

The aberrant NMJ morphology in *fsn-1* animals was confirmed by serial electron microscopy section, tracing and reconstruction of 17 μm (wild-type) and 38 μm (*fsn-1*) GABAergic (Figure 1K) and cholinergic (Supplementary Figure S3A) motor neurite length (Materials and methods). Wild-type adults exhibited regularly relatively spaced GABAergic NMJs (arrows, Figure 1K; 15 synapses) and cholinergic NMJs (arrows, Supplementary Figure S3A; 18 synapses), shown as abrupt swellings filled with synaptic vesicles along motor neuron axons. In *fsn-1* animals, similar to those observed in *rpm-1* (Zhen *et al*, 2000), both GABAergic (Figure 1K; 11 synapses) and cholinergic (Supplementary Figure S3; 15 synapses) motor neurons exhibited aberrantly large and small synapses that resulted in a broader distribution of synapse volume (Figure 1L, Supplementary Figure S3B).

fsn-1 mutants exhibit reduced spontaneous synaptic transmission frequency at NMJs

We examined the efficacy of synaptic transmission at NMJs by electrophysiology recording of the postsynaptic currents in the body wall muscles (Richmond and Jorgensen, 1999; Mellem *et al*, 2008; Gao and Zhen, 2011). Under our recording condition, the overall frequency of the spontaneous, miniature synaptic vesicle release events (mPSC) from both cholinergic and GABAergic NMJs (Materials and methods) was drastically reduced (~7 Hz

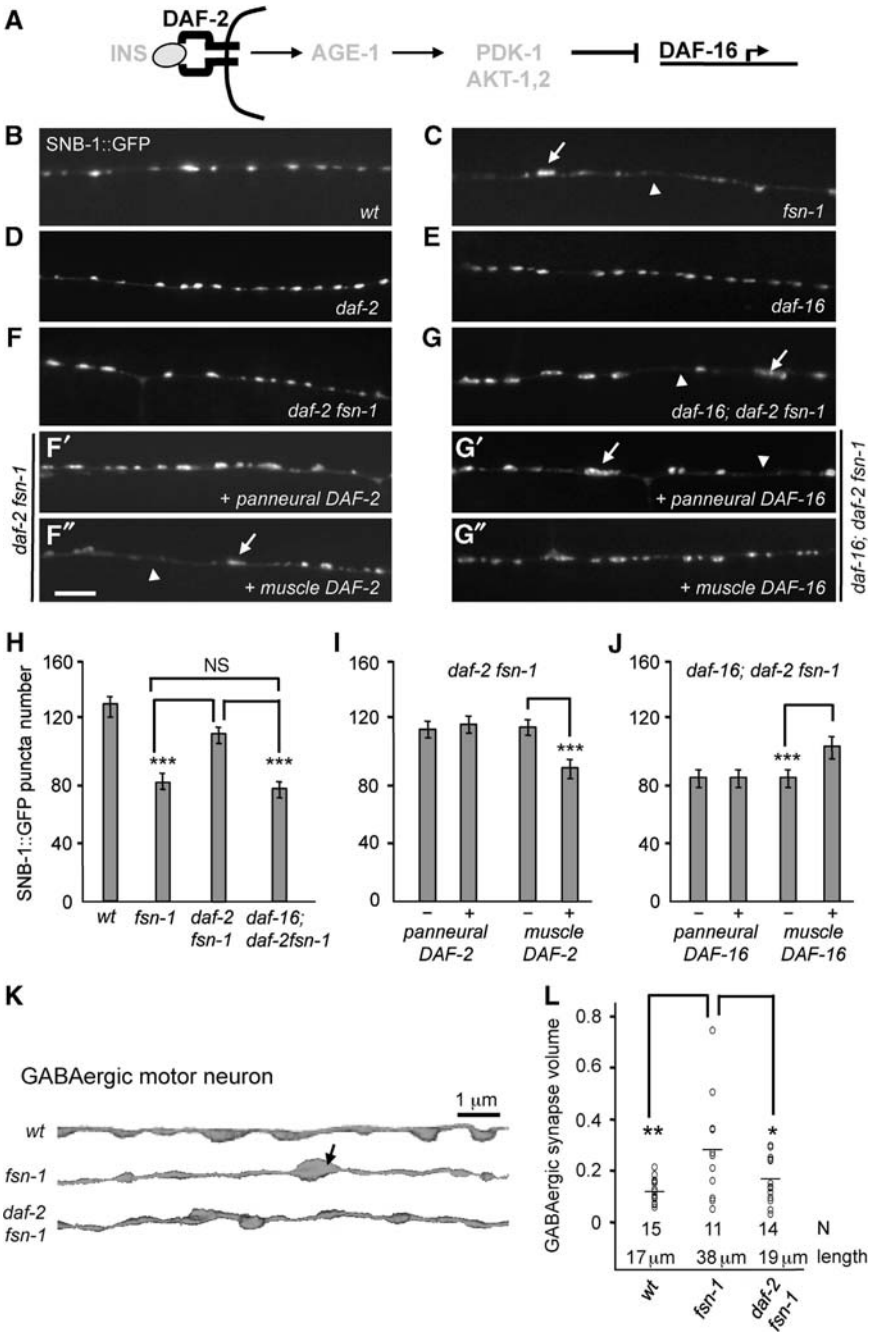

Figure 1 Reduced insulin/IGF signalling suppresses *fsn-1* synaptic defects. (**A**) A schematic representation of the canonical insulin/IGF pathway in *C. elegans*. (**B**–**G**) Representative presynaptic GABAergic NMJ morphology in animals of indicated genotypes visualized by a GABAergic SNB-1::GFP vesicle marker. Wild-type (**B**), *daf-2* (**D**) and *daf-16* (**E**) animals showed evenly spaced and round signals; *fsn-1* mutants exhibited clustered synapses (arrows) with uneven spacing (arrowheads) (**C**). *daf-2 fsn-1* showed improved morphology and spacing (**F**). When DAF-2 expression was restored panneurally (**F′**), presynaptic morphology was unaltered (**F′**), whereas restoring DAF-2 expression in the body wall muscles (**F″**) reverted the synaptic morphology to that of *fsn-1* (**F″**). *daf-16; daf-2 fsn-1* animals showed identical synapse defects as *fsn-1* animals (**G**). The presynaptic morphology was unchanged when DAF-16 was restored panneurally (**G′**), but was reverted to that of *daf-2 fsn-1* when DAF-16 was restored in muscles (**G″**). (**H**–**J**) Quantification of the total number of dorsal SNB-1::GFP puncta. Transgenic (+) and non-transgenic (−) progenies from the same *daf-2 fsn-1*(**I**) and *daf-16; daf-2 fsn-1* parent (**J**) were compared. ***$P<0.001$ by Tukey–Kramer comparison test, $N=15$ animals. (**K**, **L**) Serial EM reconstruction of the dorsal GABAergic neuron axons in wild-type, *fsn-1* and *daf-2 fsn-1* animals. Each line represents the morphology of a reconstructed motor neuron axon with *en passant* NMJs as swellings (**K**). In *fsn-1* animals, abnormally large synapses (arrows) were observed. (**L**) Scatter plot shows the distribution of synapse volume of respective genotypes. *N*, total number of synapses analysed for each genotype; length of axon analysed (in μm) was calculated from total number of sections of EM micrograph from samples of the same genotype. **$P<0.001$; *$P<0.01$; NS, $P>0.05$ by Student's *t*-test.

in *fsn-1* mutants versus ~50 Hz in wild-type animals) (Figure 2A). Excitatory (ePSC) and inhibitory (iPSC) miniature events contributed roughly equally to mPSC frequency (Hu *et al*, 2011; Hao *et al*, 2012). This indicates that the reduced mPSC frequency in *fsn-1* mutants was contributed by both cholinergic and GABAergic motor neurons (Figure 2A). Consistently, while restoration of FSN-1 expression panneurally in *fsn-1* mutants led to a full rescue of the

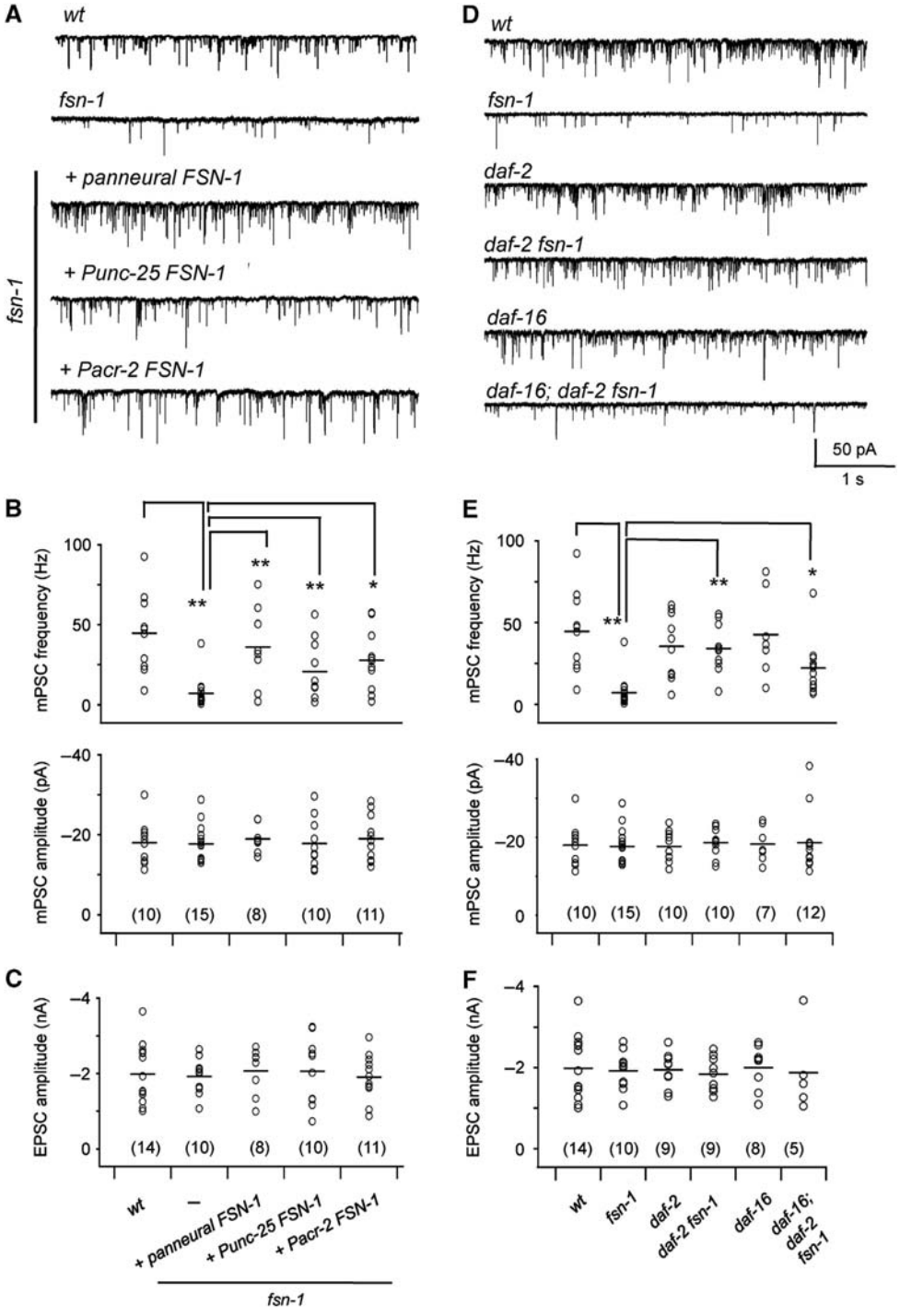

Figure 2 Spontaneous synaptic release defects in *fsn-1* animals are rescued by a partial functional loss of DAF-2/InR. (**A**) Representative traces of mPSC of wild-type animals and *fsn-1* animals expressing FSN-1 from panneural (*Prgef-1*), GABAergic (*Punc-25*) or cholinergic (*Pacr-2*) promoters. (**B**) Scatter plot of the mean mPSC frequency (top panel) and amplitude (bottom panel) of these animals. (**C**) Scatter plot of the mean EPSC amplitude of the same animals. (**D**) Representative mPSC traces of wild-type, *fsn-1, daf-2, daf-2 fsn-1, daf-16* and *daf-16; daf-2 fsn-1* animals. (**E**) Scatter plot of the mean mPSC frequency (top panel) and amplitude (bottom panel) of these animals. (**F**) Scatter plot of the mean EPSC amplitude of the same animals. Numbers in brackets indicate the number of animals recorded for each genotype. $^{*}P<0.05$, $^{**}P<0.001$ by Mann–Whitney two-tail test.

mPSC frequency (Figure 2A), an expression of FSN-1 in cholinergic (*Pacr-2*) or GABAergic (*Punc-25*) motor neurons alone partially improved mPSC frequency. Thus, FSN-1 can function through both GABAergic and cholinergic motor neurons to increase the mPSC frequency.

The mean amplitudes of mPSC (Figure 2B) were unaffected in *fsn-1* mutants. The evoked excitatory postsynaptic currents (EPSCs) (Figure 2C) were also indistinguishable between *fsn-1* and wild-type animals. This is consistent with *fsn-1* animals exhibiting grossly normal locomotion. Together, these results suggest a compromised NMJ maturation for a fraction of NMJs in *fsn-1* mutants. While the synaptic function is compromised at some NMJs of *fsn-1* mutants, there are likely robust compensatory

mechanisms in *C. elegans* that allow relatively wild-type locomotion in *fsn-1* animals.

Reducing insulin/IGF signalling improves the NMJ morphology of fsn-1 mutants

Synaptic defects exhibited by the *fsn-1* E3 ligase mutants reflect the consequence of the hyperactivation of signalling pathways that are negatively regulated by FSN-1. Decreasing such signalling activities when the FSN-1 E3 ligase function is compromised should result in partial, or full, restoration of synaptic morphology and/or transmission defects exhibited by *fsn-1*. The DLK kinase, and the downstream MAPK signalling, was uncovered as a target, and signalling event negatively regulated by the Phr E3 ligase through this approach (Nakata *et al*, 2005; Collins *et al*, 2006).

To identify additional signalling pathways that contribute to synapse development in a FSN-1-dependent manner, we examined genetic interactions between *fsn-1* and several signalling mutants, including those for DAF-2 (insulin/IGF), DAF-4 (TGF-β), CAM-1(ROR/Wnt), EGL-15(FGF), LET-23(EGF) and VAB-1(Eph). *daf-2* was identified as the only robust suppressor of *fsn-1*. DAF-2, the sole insulin/IGF receptor in *C. elegans*, is essential for embryonic and larval development (Kenyon *et al*, 1993; Kimura *et al*, 1997). The canonical, partial loss-of-function *daf-2(e1370ts)* allele is viable, and exhibited no observable defects in NMJ morphology (Figure 1D). However, the *daf-2* mutation robustly suppressed NMJ defects exhibited by *fsn-1* mutants. To bypass developmental arrest, *daf-2(e1370ts)fsn-1* mutants were maintained under permissive temperature until the L4 larval stage, and phenotype analysed in adults (Materials and methods). At GABAergic NMJs, *daf-2 fsn-1* mutants exhibited a significant increase in the presynaptic SNB-1::GFP number (to ∼90% of the wild-type level) (Figure 1H), and an improved morphology, where they appear discrete and even-sized (Figure 1F). Concomitantly, in *daf-2 fsn-1* mutants, the number of postsynaptic $GABA_R$::GFP clusters was increased and the morphology became more uniform (Supplementary Figure S1). The restored, more evenly sized and distributed cholinergic and GABAergic NMJs in *daf-2 fsn-1* animals was further confirmed by the expression patterns of endogenous $GABA_R$/UNC-49, VAChT/UNC-17 and ACh_R/UNC-38 (Supplementary Figure S1), as well as by EM reconstruction (Figure 1K and L, 14 GABAergic NMJs; Supplementary Figure S3, 14 Cholinergic NMJs). Two additional *daf-2* conditional alleles (*m577ts* and *e1368ts*) also showed partial rescue of *fsn-1*'s GABAergic synapse defect, but to a less degree than *e1370* (Supplementary Figure S4). Both are weaker alleles for the constitutive dauer phenotype (Gems *et al*, 1998; Supplementary Figure S4); their effect on *fsn-1* synaptic defects thus correlated with the degree of DAF-2's functional loss (Supplementary Figure S4). The canonical *daf-2* allele was used for the rest of the study.

Activation of DAF-2/InR triggers the sequential activation of PI-3 kinase AGE-1, PI-3-dependent kinase PDK-1, and functionally redundant kinases AKT-1 and AKT-2 (Kenyon *et al*, 1993; Morris *et al*, 1996; Kimura *et al*, 1997; Paradis and Ruvkun, 1998; Paradis *et al*, 1999). Like DAF-2, AGE-1 and PDK-1 are essential during development. Viable, partial loss-of-function *age-1* and *pdk-1* mutants also exhibited a partial suppression of the reduced synapse number and aberrant synapse morphology in *fsn-1* (Supplementary Figure S2B and C). *fsn-1; akt-1* and *fsn-1; akt-2* animals only exhibited moderately increased synapse number (Supplementary Figure S2C); but we did not test the effect of *akt-1; akt-2* due to their requirement for viability (Paradis and Ruvkun, 1998).

The canonical activation of insulin/IGF signalling ultimately leads to the phosphorylation and inhibition of the FOXO transcription factor DAF-16 (Ogg *et al*, 1997; Lee *et al*, 2001; Lin *et al*, 2001). *daf-2*-mediated suppression of *fsn-1* synaptic morphology defects requires DAF-16. *daf-16(mu86)*, a deletion allele that affects all known *daf-16* isoforms (Lin *et al*, 2001), did not exhibit overt NMJ defects (Supplementary Figures S1 and S2C). The loss of *daf-16*, however, reverted *daf-2*-mediated suppression. *daf-16; daf-2 fsn-1* triple mutants reverted to a phenotype fully resembling *fsn-1* animals: the number of GABAergic pre- (SNB-1::GFP, Figure 1H) and postsynaptic ($GABA_R$::GFP, Supplementary Figure S1A) markers were reduced; endogenous GABAergic and cholinergic synaptic proteins became unevenly distributed (Supplementary Figure S1).

DAF-2/DAF-16-signalling cascade-mediated modification of synapse phenotype is specific for *fsn-1* mutants. While *rpm-1* mutants exhibit similar characteristic synaptic defects as *fsn-1* animals, *daf-2; rpm-1* animals did not exhibit significant improvement in NMJ morphology (Figure 8A). These results argue against insulin/IGF signalling being a general modifier of synapse development, but rather, are in favour of a possibility that a failure in attenuation of insulin/IGF signalling contributes more specifically to the NMJ defects of *fsn-1* mutants.

Reducing insulin/IGF signalling increases mPSC frequency of fsn-1 mutants

Improved NMJ morphology in *daf-2 fsn-1* animals also coincided with a partial increase of mPSC frequency by electrophysiology analyses (Figure 2D and E). While the loss of DAF-16 alone did not affect mPSC frequency, *daf-16; daf-2 fsn-1* animals exhibited a significantly decreased mPSC frequency, reverting the suppressive effect of *daf-2* (Figure 2D and E). Unlike the case in NMJ morphology, however, the mPSC frequency of *daf-16; daf-2 fsn-1* was not fully reduced to the *fsn-1* level; therefore additional DAF-2 effectors may also contribute to a reduced mPSC frequency in *fsn-1* mutants. Taken together with the NMJ morphology data, these results imply that an increased canonical insulin/IGF-signalling activity contributes to synapse defects associated with the functional loss of FSN-1. Moreover, the FOXO/DAF-16 transcription factor is a major, but unlikely the sole, effector of insulin/IGF signalling that modulates NMJ development and functional maturation.

A postsynaptic requirement for insulin/IGF signalling during synapse development

Components of the DAF-2/DAF-16-signalling cascade are ubiquitously expressed in *C. elegans* (Kimura *et al*, 1997; Ogg *et al*, 1997; Paradis and Ruvkun, 1998; Paradis *et al*, 1999). To determine where the DAF-2/DAF-16-signalling cascade exerts its modulatory effects on *fsn-1* phenotypes, we restored DAF-2 or DAF-16 expression by either a panneural (*Prgef-1*), or a muscle-specific promoter (*Pmyo-3*) in *daf-2 fsn-1* or *daf-16; daf-2 fsn-1* mutants, respectively, and quantified their effects by the presynaptic GABAergic NMJ marker.

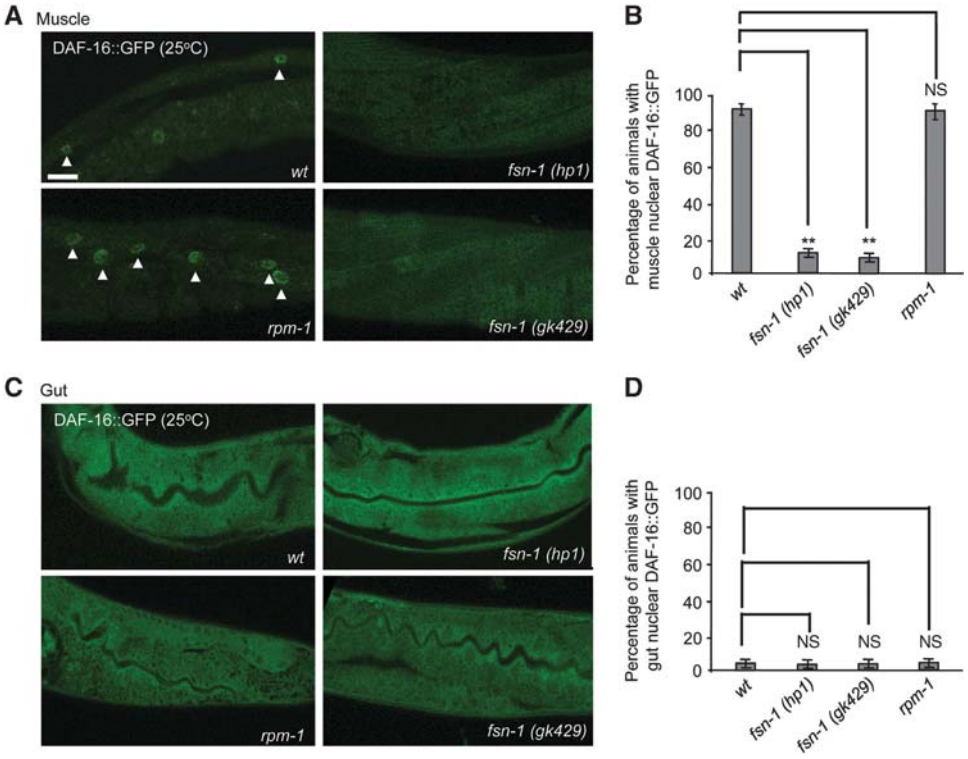

Figure 3 Insulin signalling is increased in *fsn-1* mutant. (**A**) Representative confocal images of wild-type (wt), *fsn-1(hp1* and *gk429)* and *rpm-1* animals carrying DAF-16::GFP (*muIs71*) transgene. Arrowheads indicate muscle nuclei with DAF-16::GFP. Animals were cultured at 25 °C and fixed with paraformaldehyde before imaging. (**B**) Quantification of animals in **A** with nuclear DAF-16::GFP in muscle cells. At least 90 animals were counted for each strain in a single trial, and experiment was repeated three times. (**C**) Confocal images of animals with same genotypes as in **A** but focusing on DAF-16::GFP in the gut. (**D**) Quantification of animals in **C** with gut nuclear DAF-16::GFP. Statistical analysis was done by Tukey–Kramer comparison test. $^{**}P > 0.001$.

We constructed a functional DAF-2 mini-gene that fully rescued *daf-2*'s dauer defects when expressed pan-tissuely (Materials and methods; manuscript in preparation). Panneural expression of the DAF-2 mini-gene in *daf-2 fsn-1* animals failed to revert the *daf-2*-mediated suppression of *fsn-1* synapse defects (Figure 1F′). By contrast, expressing DAF-2 in body wall muscles fully reverted the synapse morphology in *daf-2 fsn-1* to that of *fsn-1* mutants (Figure 1F″).

Three main DAF-16 isoforms, DAF-16a, DAF-16b and DAF-16d/f (Kwon *et al*, 2010; Lin *et al*, 2001), were tested for their ability to revert the effect of *daf-16(mu86)*. Restoring the expression of a functional DAF-16a mini-gene (Materials and methods; manuscript in preparation), but not other isoforms, in body wall muscles led to rescued synapse morphology and increased synapse number, similar to *daf-2 fsn-1* mutants (Figure 1G″ and J; Supplementary Methods). By contrast, when expressed in the nervous system, DAF-16a failed to alter the synaptic morphology and number in *daf-16; daf-2 fsn-1* mutants (Figure 1G′ and J). Therefore, at the GABAergic NMJ, the DAF-2/DAF-16-signalling cascade functions in the postsynaptic muscles to affect synapse development. This contrasts the case for FSN-1, which is expressed exclusively in the nervous system and is required in presynaptic neurons to regulate GABAergic NMJ development (Liao *et al*, 2004).

A moderate increase in postsynaptic insulin-signalling activity in fsn-1 mutants

Reducing the postsynaptic DAF-2/DAF-16 signalling suppresses GABAergic NMJ defects of *fsn-1*, suggesting that the loss of *fsn-1* function may lead to an increase in insulin-signalling activity. Since the activation of insulin signalling prevents DAF-16 nuclear translocation (Ogg *et al*, 1997), we examined the subcellular localization of *muIs71*, a functional DAF-16a::GFP reporter (Lin *et al*, 2001) in muscle cells, as an indirect measure for insulin-signalling activity. DAF-16a::GFP signals were fixed prior to imaging, since in live animals, they exhibited robust nuclear translocation during imaging (see Materials and methods).

At 25°C, while we observed muscle nuclear DAF-16::GFP in >90% wild-type animals, only ~10% *fsn-1* mutants accumulated DAF-16::GFP in muscle nucleus (Figure 3A and B). *muIs71* also expresses detectable level of GFP signals in the intestine. In the same set of animals, intestinal DAF-16::GFP signals remained mostly cytoplasmic, and non-distinguishable between wild-type animals and *fsn-1* mutants even at 25 °C (Figure 3C and D). These observations indicate that the loss of *fsn-1* function coincides with a moderate increase in insulin-signalling activity in muscle cells. *rpm-1* mutants showed a similar degree of nuclear DAF-16::GFP as wild-type animal (Figure 3A and B), supporting that RPM-1 does not function in the same pathway as FSN-1 in affecting insulin-signalling activity.

INS-4 and INS-6 are neuronal, agonistic DAF-2/InR ligands

Because both DAF-2 and DAF-16 are required in muscles, and FSN-1 functions through neurons, we examined the possibility that FSN-1 attenuates postsynaptic DAF-2/DAF-16

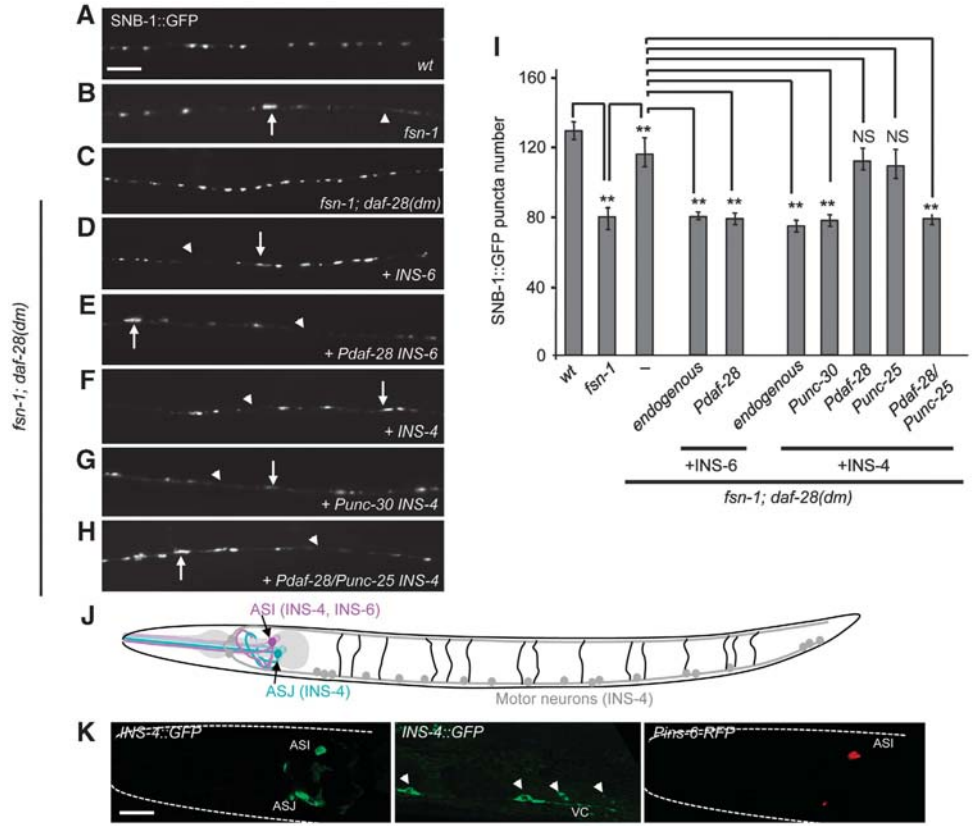

Figure 4 INS-4 and INS-6 are agonistic DAF-2 ligands for synapse development. (**A**–**H**) Representative presynaptic morphology of GABAergic NMJs visualized by the SNB-1::GFP vesicle marker in wild-type (**A**), *fsn-1* (**B**), *fsn-1; daf-28(dm)* animals (**C**) and *fsn-1; daf-28(dm)* animals overexpressing INS-6 driven by its endogenous (**D**) or *daf-28* promoter (**E**) and *fsn-1; daf-28(dm)* animals with INS-4 overexpressed from its endogenous (**F**) *unc-30* (**G**) or *daf-28* + *unc-25* promoters (**H**). Abnormal clustering (arrows) and spacing (arrowheads) of synapses were observed in *fsn-1* and *fsn-1; daf-28(dm)* animals overexpressing INS-4 or INS-6. (**I**) Quantification of total dorsal SNB-1::GFP punctum number in animals analysed in **A**–**H**, $**P<0.001$, NS $P>0.05$ by Tukey–Kramer comparison test, $N=15$ animals. (**J**) Schematic representation of *C. elegans* nervous system showing the location of ASI, ASJ sensory neurons and motor neurons. (**K**, left and middle panels) INS-4::GFP driven by its own promoter and 3′ UTR shows expression in ASI and ASJ neurons plus some motor neurons along the ventral nerve cord (VC). Punctate fluorescent signals were observed along neurites of the ventral nerve cord. Motor neurons are denoted by arrowheads. (**K**, right panel) A transcriptional RFP reporter of *ins-6* shows expression in ASI neuron. Scale bar: 5 μm.

signalling through affecting neuronal insulin/IGF-like ligands for DAF-2/InR. In this scenario, the loss of function of agonistic DAF-2 ligands should mimic the suppressive effect of *daf-2* mutants on *fsn-1*.

We systematically examined the genetic interaction between *fsn-1* and the available 35 deletion mutants for the 40 *C. elegans* insulin/IGF-encoding genes (Pierce *et al*, 2001; Li *et al*, 2003). None of the double mutants exhibited a significant rescue of *fsn-1* synapse defects (Supplementary Table S1). This is consistent with the previous finding that multiple insulin/IGF-like ligands function redundantly to activate DAF-2 in order to prevent constitutive dauer formation (Pierce *et al*, 2001; Li *et al*, 2003). Indeed, while the deletion mutant for an insulin-like ligand DAF-28, *daf-28(lf)*, did not modify the *fsn-1* synapse defects (Supplementary Figure S5), a dominant-negative allele, *daf-28(dm)*, which constitutively activates dauer formation through inhibiting multiple *ins* ligands (Li *et al*, 2003), robustly suppressed synaptic morphology defects exhibited by *fsn-1* animals (Figure 4C, Supplementary Figure S5D). *ins*-mediated suppression of *fsn-1* synapse defect is dependent on the canonical insulin/IGF signalling: *daf-16; fsn-1; daf-28(dm)* animals exhibited similar synaptic defects as *fsn-1*.

The large number of *ins* genes, many of which are tightly clustered (for example, *ins-4*, *ins-5* and *ins-6* are situated within a 4.7-kb genomic region), makes it difficult to systematically examine the effect of double or triple *ins* mutant combinations. Overexpression of single *ins* genes in *daf-28(dm)* to revert the constitutive dauer phenotype led to the identification of a fraction of agonistic DAF-2 ligands that prevent dauer formation (Li *et al*, 2003). We took an analogous approach to identify *ins* ligands that affect synapse development and overexpressed all insulin-like ligands in *fsn-1; daf-28(dm)* animals. While overexpression of INS-2, INS-3, INS-4 or INS-6 individually all suppressed the constitutive dauer phenotype of *fsn-1; daf-28(dm)* (Supplementary Figure S5), only INS-4 or INS-6 overexpression, driven by either a panneural promoter or their endogenous promoters, reverted the synaptic phenotype of *fsn-1*; *daf-28(dm)* to that of *fsn-1* (Figure 4C, D and F, Supplementary Figure S5).

We determined that INS-4 and INS-6 are expressed by, and functionally required in, sensory and/or motor neurons to modify the NMJ morphology of *fsn-1; daf-28(dm)*. As recently reported (Cornils *et al*, 2011), *Pins-6*-RFP signals were restricted to the ASI sensory neurons under normal conditions (Figure 4K), and switched to the ASJ sensory

neurons upon starvation (Cornils *et al*, 2011). INS-6 expression from these sensory neurons alone (Figure 4E, *Pdaf-28*-INS-6) fully reverted the GABAergic NMJ morphology of *fsn-1; daf-28(dm)* to that of *fsn-1*.

INS-4, on the other hand, is required for both sensory and motor neurons to affect synapse development. Constitutive and robust INS-4::GFP and *Pins*-4-RFP signals were observed in the ASI and ASJ sensory neurons, while weaker signals were also detected in ventral cord motor neurons, including GABAergic neurons (Figure 4K). To determine whether an expression in these neurons is necessary for INS-4 function, we expressed INS-4 in ASI/ASJ (*Pdaf-28*), GABAergic motor neurons (*Punc-25*), ASI + GABAergic neurons (*Punc-30*; Supplementary Figure S6) and ASI/ASJ + GABAergic neurons (*Pdaf-28* + *Punc-25*). INS-4 expression from both ASI and GABAergic motor neurons (*Punc-30*, or, *Pdaf-28* + *Punc-25*) was required for a full reversion of the GABAergic NMJ morphology of *fsn-1; daf-28(dm)* to that of *fsn-1* (Figure 4F–I).

These results suggest that INS-4 and INS-6 are agonistic DAF-2 ligands secreted by both sensory and motor neurons to modulate postsynaptic DAF-2/DAF-16 signalling, and to affect NMJ development. Consistently, panneural co-overexpression of INS-4 and INS-6 in wild-type animals led to a reduced number of GABAergic NMJs and aberrant morphology that were characteristic of, albeit being milder than, those exhibited by *fsn-1* animals (Supplementary Figure S7).

PC2/EGL-3 processes INS-4 and INS-6

Mammalian insulin is synthesized as a pre-proinsulin precursor, and processed by multiple PCs to release mature insulin. Among the 40 *C. elegans* insulin/IGF-like ligands, only INS-18 and INS-1 exhibit the canonical B–C–A peptide configuration, whereas the rest contain contiguous A and B peptides. Among them, eight, including INS-4 and INS-6, contain an additional F-peptide (Pierce *et al*, 2001; Li *et al*, 2003). Whether these ligands undergo processing and the responsible PCs are unknown.

INS-4 and INS-6 were classified as furin-processed ligands (Li *et al*, 2003). Their predicted cleavage sites for their F-peptides (R51R52 and R57R58, respectively), however, resemble that of the PC2-processed C–A junction (RR motif) of the mammalian insulin. Mutating the respective RR to AA in both INS-4::GFP and INS-6::GFP resulted in a reduced mobility shift that corresponds to the predicted molecular weight of an unprocessed F–B–A::GFP product in wild-type animals (Figure 5A), supporting that both INS-4 and INS-6 are likely processed by PC2.

To identify the PC responsible for INS-4 and INS-6 processing, we compared the mobility of INS-4::GFP and INS-6::GFP in the loss-of-function mutants for all *C. elegans* PCs, with those of their non-cleavable forms. Mutating the respective RR to AA in either INS-4::GFP or INS-6::GFP resulted in a reduced mobility shift that corresponds to the predicted molecular weight of an unprocessed F–B–A::GFP product in wild-type animals (Figure 5A). In *egl-3*, but not in any other PC mutants, *kpc-1, bli-4* and *aex-5*, wild-type INS-4::GFP and INS-6::GFP exhibited a similar migration pattern as the non-cleavable INS-4(AA)::GFP and INS-6(AA)::GFP (Figure 5A). As an additional control, INS-22::Venus, an *ins* ligand not requiring additional processing after the removal of the signal peptide, did not show mobility shift in *egl-3* mutants (Figure 5B).

Lastly, EGL-3-dependent INS-4 and INS-6 processing is necessary for their modulation on synapse morphology. Overexpression of either INS-4(AA) or INS-6(AA) completely failed to revert the rescuing effect exhibited by *fsn-1; daf-28(dm)* (Figure 5C). Taken together, PC2/EGL-3 is responsible for INS-4 and INS-6 processing and required for their functional maturation to modulate synapse development.

Functional loss of EGL-3 in INS-4- and INS-6-expressing neurons improves NMJ morphology and function in fsn-1 mutants

Affecting the maturation of multiple neuronal insulin/IGF-like ligands that modulate synapse development, EGL-3 is poised to affect postsynaptic insulin/IGF signalling. This prompted us to examine whether altering *egl-3* activity modifies the synaptic defect of *fsn-1*. *egl-3* deletion mutations (data shown for the *ok979* allele only) led to increased GABAergic NMJ number and improved morphology in *fsn-1; egl-3* animals (Figure 6A′ and A″). This suppressive effect was also dependent on the presence of DAF-16 (Figure 6A‴). Importantly, similar to *daf-2, egl-3* loss-of-function mutations increased the mPSC frequency of *fsn-1* animals (Figure 6D and E). The loss-of-function mutations in other *C. elegans* PCs, *kpc-1, bli-4* and *aex-5,* did not lead to a suppression of *fsn-1* synaptic morphology defects (Figure 5D). We noted that the rescuing effect of *egl-3* on both the morphology and synaptic transmission of *fsn-1* was qualitatively weaker than that of *daf-2* (Figure 6C and E), suggesting the involvement of additional insulin-like ligands.

EGL-3 is expressed broadly in the nervous system (Kass *et al*, 2001). Restoring the expression of EGL-3 by a panneural promoter, but not by a muscle promoter, fully reverted the suppressive effect on GABAergic NMJ in *fsn-1; egl-3* animals (Figure 6B and C). Importantly, specific restoration of EGL-3 in INS-4 and INS-6-expressing neurons (*Punc-30* for ASI + GABAergic motor neurons, or, *Pdaf-28* + *Punc-25* for ASI/ASJ + GABAergic motor neurons) in *fsn-1; egl-3* animals led to a full reversion of the GABAergic NMJ number and morphology to that of *fsn-1* (Figure 6B and C).

In addition to INS-4 and INS-6, EGL-3 processes FMRFamide-like (*flp*) and neuropeptide-like proteins (*nlp*) neuropeptides (Li *et al*, 1999; Pierce *et al*, 2001; Li *et al*, 2003; Husson *et al*, 2005). Could EGL-3's role in synapse development also involve these neuropeptides? The maturation of a majority of *flp* and *nlp* requires a carboxypeptidase E/EGL-21 to remove the C-terminal basic residues after EGL-3 processing (Husson *et al*, 2006). If EGL-3's role in synapse development also involves non-*ins* neuropeptides, *egl-21* should exhibit a similar modifying effect on the synaptic defects of *fsn-1* mutants. However, the loss of EGL-21 function did not suppress the synaptic defect of *fsn-1* mutants (Figure 5D). These results further support that multiple neuronal *ins* peptides, including INS-4 and INS-6, processed by EGL-3, and the subsequent insulin/IGF signalling contributes to FSN-1-mediated regulation of synapse development.

FSN-1 interacts with, and ubiquitinates, EGL-3 in vitro

Next, we investigated if FSN-1 may negatively regulate EGL-3 through targeting it for ubiquitination. We first used

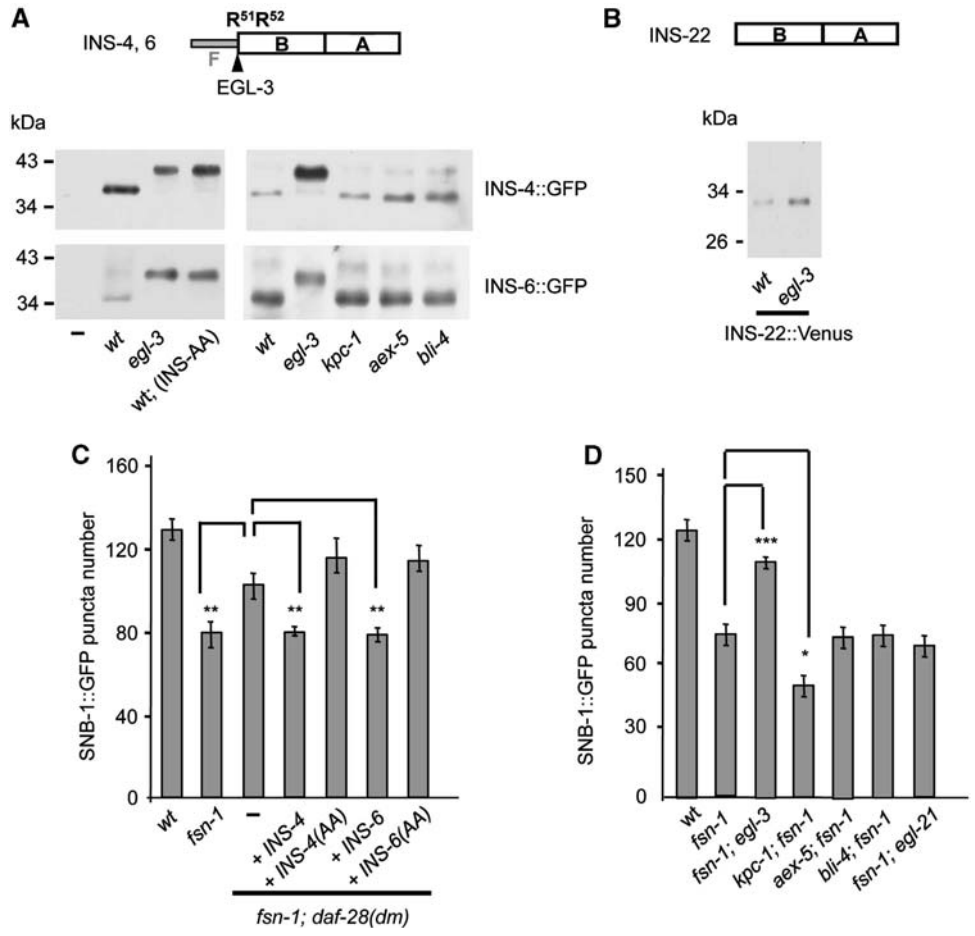

Figure 5 EGL-3 processes INS-4 and INS-6. (**A**) (Top) A schematic diagram of the structure of *C. elegans* INS-4 and INS-6. (Bottom panels) Western blotting analyses of panneurally expressed INS-4::GFP and INS-6::GFP and their non-cleavable forms INS(AA)::GFP in wild-type (wt) and *egl-3* animals, and wild-type INS-4::GFP and INS-6::GFP in *kpc-1, aex-5* and *bli-4* animals. Non-transgenic, wild-type animals were negative controls (−). (**B**) Western blot analyses with lysates from wild-type (*wt*) or *egl-3* animals expressing INS-22::Venus. (**C**) Quantification of total SNB-1::GFP puncta number on dorsal nerve cord in wild-type, *fsn-1*, *fsn-1; daf-28(dm)* and *fsn-1; daf-28(dm)* overexpressing INS-4, INS-6, uncleavable INS-4(AA) or INS-6(AA) by a panneural promoter. (**D**) Quantification of the total dorsal SNB-1::GFP puncta number in animals with indicated genetic backgrounds. Only *egl-3* mutants exhibited suppression of *fsn-1* defects. $***P<0.001$, $**P<0.01$, $*P<0.05$ by Tukey–Kramer comparison test, $N=15$ animals.

a heterologous expression system to examine if co-transfected FSN-1::FLAG and EGL-3::HA could directly interact. Immunoprecipitation of FSN-1::FLAG readily pulled down EGL-3::HA. The reciprocal immunoprecipitation of EGL-3::HA only effectively brought down FSN-1::FLAG in the presence of a proteosome inhibitor MG132 (Supplementary Figure S8A). These results support that co-transfected FSN-1::FLAG and EGL-3::HA are present in the same protein complex in HEK293T cells. The observation that the FSN-1–EGL-3 interaction was stabilized by proteasome inhibitors suggests that the fraction of EGL-3 associated with FSN-1 was prone to degradation.

We identified protein motifs necessary for FSN-1 and EGL-3 interaction. FSN-1 consists of an F-box and a SPRY domain. EGL-3::HA co-immunoprecipitated with full-length FSN-1 (FL) and FSN-1 without the F-box domain (ΔF), but not with FSN-1 missing the SPRY domain (ΔS) (Supplementary Figure S8B). A similar deletion analysis for EGL-3 revealed that its C-terminal 150 amino acids were both necessary and sufficient to mediate the interaction with FSN-1::FLAG (Supplementary Figure S8C).

PCs are localized mainly to the Golgi apparatus and associate with lipid rafts (Villeneuve *et al*, 2000; Uehara *et al*, 2001). The membrane topology of mammalian PC remains slightly controversial (Stettler *et al*, 2005). Additional studies are needed to determine whether EGL-3 and FSN-1 interact with each other directly, or through other proteins. If they interact directly, these results are more consistent with EGL-3's C terminus exposed to the cytosol, which is necessary for FSN-1 binding.

To determine if FSN-1 promotes EGL-3 ubiquitination in HEK293T cells, Myc-tagged ubiquitin was co-transfected with EGL-3::HA to aid the detection of its ubiquitination. In the absence of FSN-1::FLAG, we observed a basal level, Myc-positive high molecular weight fraction of immunoprecipitated EGL-3::HA (Figure 7A), a typical pattern of multi-ubiquitinated proteins. The basal level of ubiquitination indicates the presence of endogenous protein machineries that target EGL-3 for ubiquitination in HEK293T cells. The level of ubiquitinated EGL-3::HA was significantly increased when FSN-1::FLAG was co-transfected (Figure 7A). As a negative control, Sprouty, an unrelated *Drosophila*

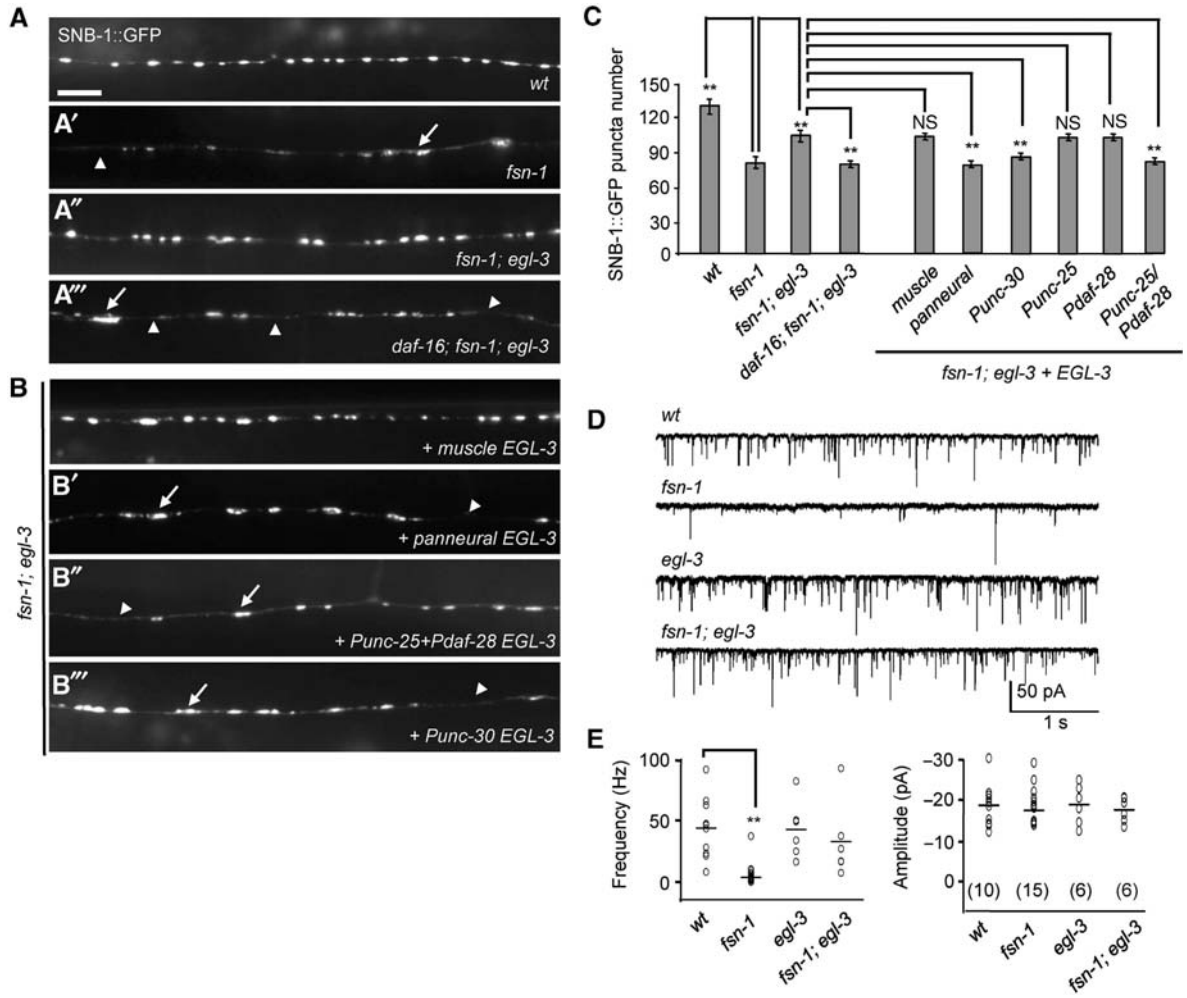

Figure 6 A functional loss of PC2/EGL-3 in INS-4 and INS-6-producing neurons leads to partial suppression of *fsn-1* synaptic defects. (**A**–**B**) Representative presynaptic morphology of GABAergic NMJs in wild-type (**A**), *fsn-1*(**A**′), *fsn-1; egl-3* (**A**″), *daf-16; fsn-1; egl-3* (**A**‴) animals, and *fsn-1; egl-3* animals with EGL-3 expression restored in muscles (**B**), panneural (**B**′), ASI+ GABAergic (*Punc-30* (**B**″), *Punc-25*+*Pdaf-28* (**B**‴)) neurons. (**C**) Quantification of the total dorsal SNB-1::GFP number in animals with indicated genotypes. $^{**}P<0.001$ by Tukey–Kramer comparison test. $N=15$ animals. (**D**) Representative traces of mPSC in wild-type, *fsn-1*, *egl-3* and *fsn-1; egl-3* animals. (**E**) Scatter plots of the mean mPSC frequency and amplitude of animals from **D**. Number in bracket shows the number of animals recorded.

protein of a molecular weight similar to EGL-3::HA, did not exhibit detectable ubiquitination in either the absence or presence of FSN-1::FLAG (Figure 7A).

The increased ubiquitination of EGL-3 was FSN-1-dependent. We isolated a missense mutation allele of *fsn-1, hp2*, where the loss-of-function mutation (R191C) did not affect the stability of FSN-1 (Supplementary Figure S9B), but resulted in the same degree of synaptic defects as two null alleles (Supplementary Figure S9A). FSN-1(*hp2)*::FLAG drastically reduced its interaction with EGL-3::HA in co-transfected HEK293 cells when compared to wild-type FSN-1::FLAG (Supplementary Figure S9C). FSN-1(*hp2*)::FLAG failed to increase EGL-3::HA ubiquitination (Figure 7A). Therefore, FSN-1 specifically enhances EGL-3 ubiquitination.

Multiple N-terminal truncated forms of EGL-3, which retained their ability to interact with FSN-1 (Supplementary Figure S6C), also exhibited multi-ubiquitination (Figure 7B, Supplementary Figure S9D for a longer exposure) that was resolvable at single-ubiquitin increments in the low molecular weight range (Supplementary Figure S9D). Taken together, EGL-3 is targeted by FSN-1 to potentiate its ubiquitination in HEK293T cells.

FSN-1 negatively regulates EGL-3::GFP level in vivo

EGL-3 is targeted by FSN-1 for ubiquitination *in vitro*, supporting a notion that FSN-1 may regulate synaptic development in part through EGL-3. To address if FSN-1 may regulate EGL-3 *in vivo*, we compared the protein level of a functional, panneurally expressed, integrated EGL-3::GFP array between wild-type and *fsn-1* animals. We observed a two-fold increase of EGL-3::GFP in both *fsn-1* null alleles (Figure 7C and D). Similar level of EGL-3::GFP mRNA was detected from all strains by RT–PCR analyses (Supplementary Figure S10); the increase of the EGL-3::GFP protein level was thus unlikely to be caused by increased transcription.

Our *in vitro* experiments suggest that FSN-1-mediated ubiquitination of EGL-3 requires the C-terminus of EGL-3. This C-terminal region coincides with the P-domain, a motif that was hypothesized to regulate the folding,

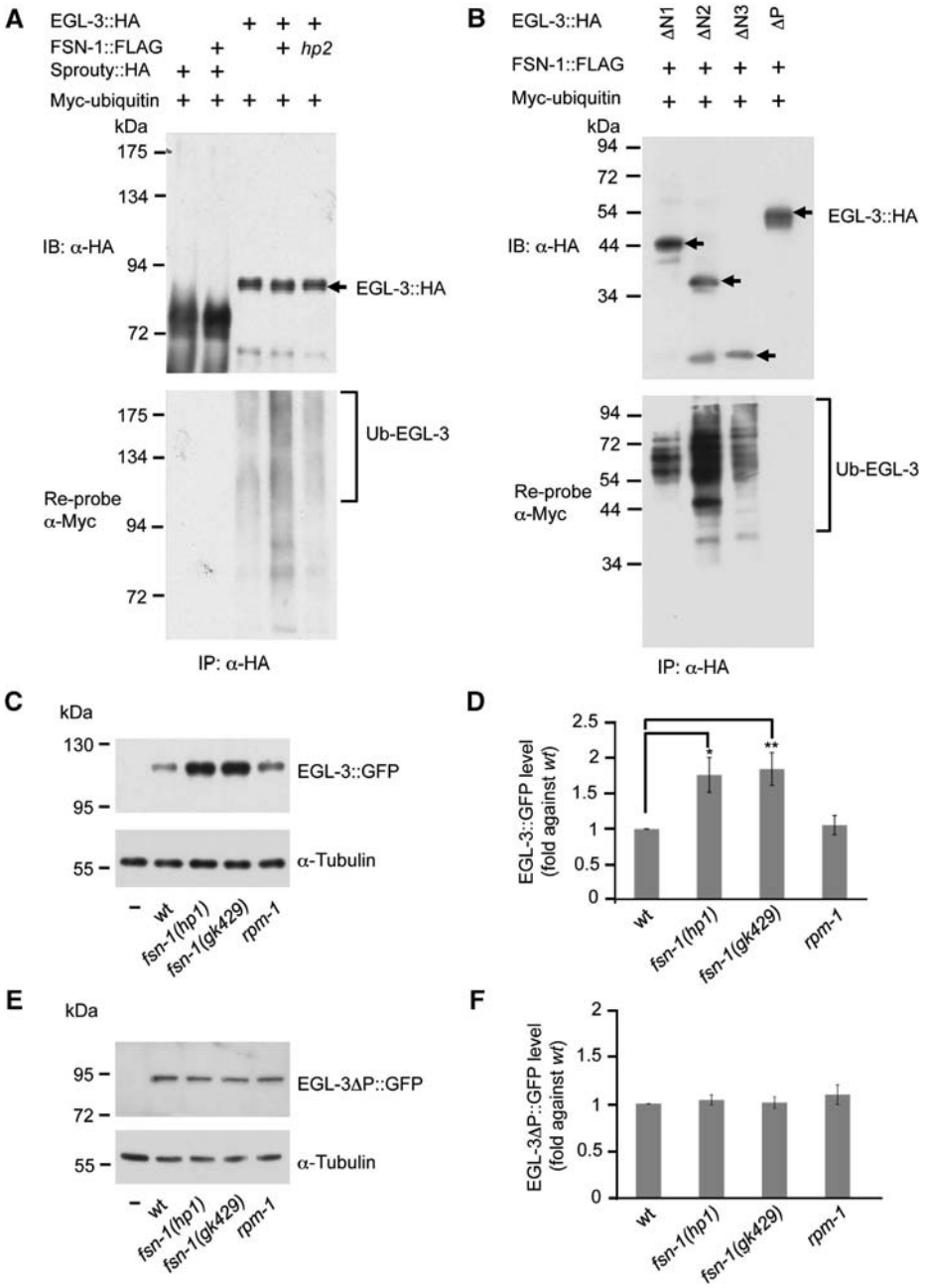

Figure 7 FSN-1 ubiquitinates EGL-3 *in vitro*, and reduces EGL-3 level *in vivo*. (**A**) FSN-1 ubiquitinates EGL-3 in HEK293T cells. EGL-3::HA or Sprouty::HA (negative control) were co-transfected with wild-type or mutant (*hp2*) FSN-1::FLAG, and Myc-ubiquitin. Immunoprecipitated EGL-3::HA or Sprouty::HA was probed with anti-HA antibodies (top panel), stripped and re-probed with anti-Myc (bottom panel) to detect the ubiquitinated fraction. (**B**) FSN-1-dependent EGL-3 ubiquitination requires the P-domain. EGL-3 deletion mutants that retain the P-domain and interaction with FSN-1 (ΔN1–ΔN3) showed multiple higher molecular weight bands (top panel) that represent ubiquitinated forms (lower panel). (**C**–**D**) Western blot analyses on *C. elegans* lysates from strains carrying the same integrated transgenic arrays expressing EGL-3::GFP (**C**) or EGL-3ΔP::GFP (**D**). Lysates from non-transgenic animals were negative controls (–). (**E**–**F**) Quantification of the level of EGL-3::GFP (**E**) and EGL-3ΔP::GFP (**F**), normalized against α-tubulin. $^{**}P<0.01$, $^{*}P<0.05$ by Tukey–Kramer comparison test. $N=6$ sets of replica. Error bars: s.e.m.

pH-/calcium-dependence or localization of PCs (Zhou *et al*, 1998; Muller *et al*, 2000; Assadi *et al*, 2004), but its *in vivo* function remains elusive. If EGL-3 is an *in vivo* target of FSN-1, EGL-3 missing the P-domain (ΔP) should no longer be subjected to regulation by FSN-1. The same panneurally driven, integrated EGL-3ΔP::GFP transgene exhibited similar protein levels between wild-type and *fsn-1* mutants (Figure 7E and F), further supporting that FSN-1 negatively regulates EGL-3 level.

Discussion

A conserved Phr/Fbxo45 E3 complex negatively regulates the DLK-activated p38 or JNK-signalling cascade at *C. elegans* and *Drosophila* NMJs and developing mouse motor neurons. Here, we demonstrate that an increase in insulin/IGF signalling also contributes specifically to defective NMJ development in *fsn-1* mutants. We propose that FSN-1-mediated synaptic development and function may also involve the

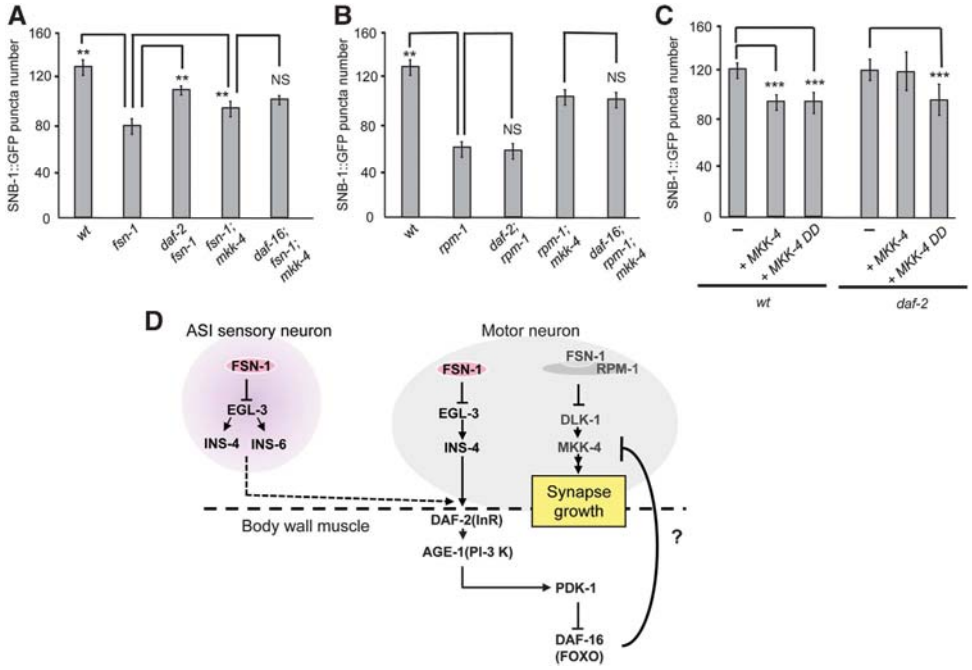

Figure 8 FSN-1 may coordinate pre- and postsynaptic signalling during synaptic development. (**A**–**B**) Genetic interactions between mutants of the insulin/IGF and p38 MAPK signalling with *fsn-1* and *rpm-1* by quantification of the dorsal SNB-1::GFP puncta number. (**A**) Both *daf-2* and *mkk-4* mutants restored the *fsn-1* synapse defect independent of the presence of DAF-16. (**B**) *daf-2* mutants did not rescue the *rpm-1* synapse defect. *mkk-4* rescued *rpm-1* synaptic defect independent of DAF-16. (**C**) Quantification of dorsal SNB-1::GFP puncta in wild-type or *daf-2* animals expressing either wild-type or constitutively active MKK-4 (DD), $^{**}P<0.01$, $^{***}P<0.001$, NS $P>0.05$ by Tukey–Kramer comparison test, $N=15$ animals. (**D**) The schematic presentation of a tentative model for FSN-1. In motor neurons, FSN-1 attenuates presynaptic MAPK with RPM-1, and postsynaptic insulin/IGF signalling independently of RPM-1. Cross-talk between these two signalling events allows axons to establish differential MAPK activity levels and to regulate synapse development at specific domains along the axon.

attenuation of insulin/IGF-signalling activity, in part, through modulating the maturation of multiple insulin-like ligands (Figure 8D).

Specificity of insulin/IGF-signalling-mediated suppression

fsn-1 NMJ defects were robustly suppressed by mutations in multiple components of the insulin/IGF-signalling pathways. Despite exhibiting similar NMJ phenotypes as the *fsn-1* mutants, none of the robust *fsn-1* suppressors in the IGF/insulin pathway exerted any obvious suppression of the synaptic defects in *rpm-1* (Figure 8A and B; data shown for *daf-2* only). A simple explanation for these results is that FSN-1 participates in negative regulation of insulin/IGF signalling largely independently of RPM-1. This notion is also consistent with the following observations: (1) *rpm-1* mutants do not exhibit decreased DAF-16::GFP nuclear localization in muscles (Figure 3B); and (2) there is no appreciable increase in EGL-3::GFP level in *rpm-1* animals (Figure 7C). Alternatively, insulin/IGF signalling may modify the synaptic defects of *fsn-1* mutants indirectly, such as through activating signalling events that are negatively regulated by FSN-1.

While *fsn-1* and *rpm-1* mutants share many phenotypic characteristics, RPM-1 can function independently of FSN-1 during axon outgrowth and axotomy-induced regeneration (Grill *et al*, 2007; Hammarlund *et al*, 2009; Grill *et al*, 2012). The present study suggests that FSN-1 may also have RPM-1-independent functions.

Insulin/IGF signalling functions genetically in parallel, or, upstream of MAPK signalling

Elevated DLK-1/Wallenda and their downstream p38/JNK MAPK activity contribute to *rpm-1/hiw* synapse defects (Nakata *et al*, 2005; Collins *et al*, 2006). The null or severe loss-of-function mutants in this MAP kinase-signalling cascade, *dlk-1*, *mkk-4* and *pmk-3*, without causing an obvious NMJ defect on their own, robustly suppressed both *rpm-1* and *fsn-1*'s synapse defects (Figure 8B). However, *mapk* mutant-mediated suppression of either *fsn-1* or *rpm-1* did not require DAF-16 (Figure 8A), indicating that MAPK signalling functions either in parallel or genetically downstream of DAF-2/DAF-16 signalling.

We attempted to distinguish these possibilities by genetic epistasis. Both *mapk* and *daf-2* mutants are strong suppressors of the *fsn-1* synapse defect (restoring the GABAergic synapse number to ~90%), making it difficult to compare their genetic interactions using the loss-of-function alleles. We thus compared the effect of a panneural MKK-4 hyperactivation between wild-type and *daf-2* animals. Overexpression of MKK-4 in wild-type animals causes a synaptic morphology defect that is abolished by the loss of its activator DLK-1. By contrast, overexpression of a constitutively activated MKK-4, MKK-4(DD), causes severe synapse defects in the absence of DLK-1 (Nakata *et al*, 2005). As reported, the number of GABAergic NMJs was severely reduced when we overexpressed either wild-type MKK-4 or MKK-4(DD) in wild-type animals (Figure 8C). Intriguingly, the effect of the same wild-type MKK-4, but not MKK-4(DD)

transgenes, was partially but consistently dampened in *daf-2(ts)* backgrounds (Figure 8C). These results are consistent with a notion that insulin/IGF signalling potentiates MKK-4 activation, but they do not exclude a possibility that insulin/IGF signalling may also function independently of activating MAPK to affect synapse development.

Differential requirement of INS-4 and INS-6 on synapse development

We identified two ligands for DAF-2/InR-mediated regulation of synapse development. INS-6 is restrictively expressed, and functionally sufficient, in the ASI and ASJ sensory neurons, whereas INS-4 expression also includes the motor neurons. Despite of its weak expression, co-restoring INS-4 in ASI and motor neurons was necessary to revert *daf-28(dm)*'s suppression on *fsn-1* synaptic defects (Figure 4). The synapse morphology in *fsn-1; daf-28(dm)* mutants did not show obvious difference in anterior versus posterior motor cord (Supplementary Figure S11). DAF-28(dm) hence has a long-range inhibitory effect on the DAF-2/InR receptor. This raises the possibility that INS-6 and INS-4 act as long-range and local activators of DAF-2, respectively.

Functional models for FSN-1

Unlike RPM-1, FSN-1 exhibits genetic interactions with both MAPK and insulin/IGF-signalling pathways. FSN-1 is therefore positioned to coordinate the cellular responses between signalling events of the developing pre- (MAPK cascade) and postsynaptic (DAF-2/DAF-16 cascade) termini. We propose two tentative functional models for FSN-1 that incorporates such a possibility (Figure 8D).

High MAPK-signalling activity inhibits synapse development and it can be regulated at multiple levels. In addition to negative regulation by FSN-1/RPM-1-mediated degradation of DLK-1, *C. elegans* sensory and motor neurons secrete multiple insulin-like ligands to regulate DAF-2/DAF-16 activity in body wall muscles. DAF-2/DAF-16 signalling modulates the secretion of unidentified factors that inhibit presynaptic MAPK, and affect NMJ development.

In the first model, FSN-1 directly regulates insulin signalling, in part, through EGL-3, which affects the maturation of both long-range and local insulin/IGFs from sensory and motor neurons (INS-4, INS-6 and others) to fine tune postsynaptic DAF-2/DAF-16 activity, and to establish the basal MAPK (and/or other signalling) activity in developing neurites. Because RPM-1 is concentrated at discrete regions (Zhen *et al*, 2000; Abrams *et al*, 2008) and FSN-1 localizes ubiquitously along *C. elegans* neuronal processes (Liao *et al*, 2004), the RPM-1/FSN-1 complex locally restricts MAPK signalling through downregulating DLK-1 to define synapse 'domains' along the axon. This model predicts that in addition to a cell autonomous function, FSN-1 can also function non-cell autonomously to affect GABAergic NMJ. Indeed, when FSN-1 was co-restored in ASI sensory neurons and cholinergic motor neurons (P*daf-28* + P*acr-2*) in *fsn-1* mutants, the defective GABAergic NMJ morphology and reduced number were partially, but consistently, rescued (Supplementary Figure S12).

In an alternative model, the modifying effect of insulin/IGF-signalling mutants is indirect. If *fsn-1* mutants exhibit a lesser degree of MAPK hyperactivation than that of *rpm-1*, their synapse defects would be more sensitive to the perturbation of MAPK activation by reducing insulin/IGF signalling. We favour the first possibility because of a fairly strong contrast in the suppression effect of insulin mutants on *fsn-1* and *rpm-1*.

In future studies, identifying retrograde signals downstream of insulin/IGF signalling and a careful examination of potential differences in insulin/IGF and MAPK-signalling activity between *fsn-1* and *rpm-1* mutants will help further dissect how FSN-1, RPM-1, MAPK and insulin/IGF signalling orchestrate synapse development.

The lack of synaptic phenotype in daf-16 null mutants

One unresolved puzzle is the lack of synapse phenotypes in *daf-16* null mutants. Because DAF-16 is a major effector of insulin/DAF-2-signalling-mediated suppression of *fsn-1* synapse defects, the simplest scenario is that *daf-16* mutants exhibit weak synaptic defects with similar characteristics as those in *fsn-1*. Instead, we could not detect obvious NMJ phenotypes, at least under our experimental conditions.

A potential explanation is that hyperactivated insulin/IGF signalling is particularly deleterious for NMJ maturation in the absence of FSN-1, whereas in wild-type animals, unknown compensative mechanisms are in place to allow NMJ development in an elevated insulin/IGF-signalling environment. DAF-16 is required for longevity of *C. elegans* (Ogg *et al*, 1997; Lin *et al*, 2001; Murphy *et al*, 2007), and its loss leads to premature neuronal aging (Pan *et al*, 2011; Tank *et al*, 2011; Toth *et al*, 2012). It will be interesting to examine whether *daf-16* mutants exhibit the synaptic defects in non-favorable conditions (genetic sensitized backgrounds, aging or stress).

Potential links between FSN-1, insulin/IGF signalling and aging

DAF-2/insulin signalling plays critical roles in longevity and aging (Kenyon *et al*, 1993; Ogg *et al*, 1997; Lee *et al*, 2001; Lin *et al*, 2001). Recent studies indicate that neuronal aging is also modulated by insulin/IGF signalling in *C. elegans* (Pan *et al*, 2011; Tank *et al*, 2011; Toth *et al*, 2012). As animals age, touch and motor neurons exhibit synapse deterioration, neurite sprouting and branching. These phenotypes are sensitive to the level of insulin/IGF signalling; decreased insulin/IGF signalling (loss of DAF-2) leads to their suppression, whereas the loss of DAf-16 either enhances these phenotypes or reverts *daf-2*'s suppression effect.

Here, we describe FSN-1-mediated regulation of insulin/IGF signalling during NMJ development. Consistent with FSN-1 attenuating insulin/IGF signalling, both alleles of *fsn-1* mutants exhibited shortened lifespan (Supplementary Figure S13). Thus an intriguing implication is that synaptic defects exhibited by *fsn-1* animals may also reflect the physiological state of the neuromuscular system undergoing stress or aging.

Materials and methods

Strains

For non-essential genes, *fsn-1, rpm-1, daf-16, egl-3, egl-21, kpc-1, aex-5, bli-4, akt-1, akt-2, dlk-1, mkk-4* and all *ins*, deletion or missense alleles predicted to cause severe loss of gene function were examined in this study. For essential genes, *daf-2, age-1* and *pdk-1*, viable, partial loss-of-function, conditional alleles were used. Deletion mutant strains were backcrossed against N2 more than three times. A full list of strains generated and used in this study is provided in Supplementary text.

Electron microscopy

One-day-old *C. elegans* adults were fixed by high pressure freezing followed by freeze substitution as described (Rostaing *et al*, 2004) with modifications (Stigloher *et al*, 2011). At least 150 serial sections (70 nm/sections) for each sample, two samples per genotype, were collected. Images of dorsal nerve cords were obtained on FEI Tecnai 20 equipped with a Gatan Dualview digital camera. Axons of the GABAergic (DD) and cholinergic (DA and DB) motor neurons were manually traced over at least 150 serial sections to identify the synapse and neuron type; the traced images were projected using the Reconstruct program (Fiala, 2005).

GABAergic and cholinergic NMJs were distinguished based on their locations in the nerve cord and their mono- and dyadic synaptic target pattern (White *et al*, 1986). NMJs are defined as large varicosities along the processes that quickly emerge while moving out of the ventral or dorsal nerve cords towards the muscle arms, and disappear when the processes 'dive' back to the nerve cords. In wild-type animals, these varicosities are associated with the appearance of synaptic and dense-core vesicles, cadherin junction-like structures with the muscle arm and a single active zone that is defined as the electron dense area at the plasma membrane surrounded by synaptic vesicles. Synapse volume is measured by multiplying the combined surface area of the cross-sections of a synapse in all sections by 70 nm.

Western blotting analysis of C. elegans lysates

Total protein lysates were prepared from mixed staged *C. elegans* cultured on NGM media as described previously (Hung *et al*, 2007). Equal amounts of lysates, adjusted against the level of α-tubulin, were analysed on western blots. Anti-GFP (Roche) was used to detect EGL-3::GFP, INS-4::GFP, INS-6::GFP, with non-transgenic N2 animals as GFP-negative controls.

Immunofluorescent staining

C. elegans were fixed and co-stained with either anti-GFP (1:200) and anti-UNC-49 (1:500) or anti-UNC-17 (1:200) and anti-UNC-38 (1:150) to detect GABAergic and cholinergic NMJs, respectively. Fixation and staining procedures were as described previously (Liao *et al*, 2004). Confocal images of stained cells and animals were acquired on a Nikon Eclipse 90i confocal microscope.

Quantification of synaptic markers

For the number of GABAergic NMJs, fluorescent puncta exhibited by GABAergic synaptic markers *juIs1* (SNB-1::GFP) and *oxIs22* (UNC-49::GFP) along the entire dorsal nerve cord were counted in 1-day young adults. For GABAergic NMJ morphology, multiple images of the same posterior region of the dorsal nerve cord in 1-day adult were captured under the same conditions by Hamamatsu digital camera on a Zeiss Axiovision microscope with a ×63 objective lens, and the acquired images processed and analysed by an in-house developed PunctaAnalyzer program and R script, as described previously (Hung *et al*, 2007). Distribution of the fluorescent punctum width was plotted as a density curve generated by Kernel Distribution Estimation Function of R program (Hung *et al*, 2007). Examiners were blinded for the genotype of animals.

Electrophysiology

Dissection and recording were carried out using protocols and solutions described in Gao and Zhen (2011) modified from Richmond and Jorgensen (1999) and Mellem *et al* (2008). One or 2-day-old hermaphrodite adults were glued to a sylgard-coated cover glass covered with bath solution. The integrity of the anterior ventral body muscle and the ventral nerve cord were visually examined via DIC microscopy, and muscle cells were patched using fire-polished 4–6 MΩ-resistant borosilicate pipettes. Membrane currents were recorded in the whole-cell configuration by a Digidata 1440A and a MultiClamp 700A amplifier, using the Clampex 10 software and processed with Clampfit 10. Data were digitized at 10–20 kHz and filtered at 2.6 kHz. The pipette solution contains (in mM): K-gluconate 115; KCl 25; $CaCl_2$ 0.1; $MgCl_2$ 5; BAPTA 1; HEPES 10; Na_2ATP 5; Na_2GTP 0.5; cAMP 0.5; cGMP 0.5, pH7.2 with KOH, ~320 mOsm. The bath solution consists of (in mM): NaCl 150; KCl 5; $CaCl_2$ 5; $MgCl_2$ 1; glucose 10; sucrose 5; HEPES 15, pH7.3 with NaOH, ~330 mOsm. Because the holding potential was at −60 mV, the mPSC frequency in this study refers to the combined spontaneous synaptic activities for both cholinergic and GABAergic NMJs. All experiments were performed at room temperatures (20–22°C).

Quantification of DAF-16::GFP signals

Animals carrying *muIs71* in different genetic backgrounds were maintained at 25 °C for one generation. Since we observed robust spontaneous nuclear localization with muscle DAF-16a::GFP in live animals when exposed to UV light, animals were washed off the plate and fixed in 5% paraformaldehyde on ice for 2 h prior to imaging and quantification (Hung *et al*, 2007). All strains were harvested and processed in parallel. The percentage of animals with nuclear GFP::DAF-16a were counted, and representative images were obtained with a Nikon Eclipse 90i confocal microscope. This experiment was repeated three times; all exhibited similar trend.

Co-immunoprecipitation and ubiquitination assay

HEK293T cells were transfected with EGL-3::HA, Myc-ubiquitin K63R (a gift from D Durocher, University of Toronto) with or without FSN-1::FLAG plasmids using Lipofectamine 2000 (Invitrogen). Myc-tagged wild-type and mutant (K48R or K63R) ubiquitins were tested for ubiquitination of EGL-3; all were able to detect enhanced ubiquitination of EGL-3::HA in the presence of FSN-1::FLAG (data not shown). K63R mutant showed the highest sensitivity for detecting ubiquitination; it was used for all experiments shown in this study. Except for experiments in Supplementary Figure S8A and D, Myc-ubiquitin (K63R) was co-transfected in all experiments in HEK293T cells, and cells were subjected to MG132 treatment.

Sixteen hours post transfection, cells were treated with 50 nM MG132. Eight hours later, cells were washed once with PBS before lysing in a lysis buffer that contains 1% NP-40, 10% glycerol, 30 mM $MgCl_2$, 50 mM Tris pH 7.4, 150 mM NaCl, 1 mM DTT, 1 mM NaF, 5 mM *N*-ethylmaleimide and complete protease inhibitor cocktail, EDTA-free (Roche). After centrifugation, equal amounts of cleared lysates were immunoprecipitated. Immunoprecipitation of FLAG-tagged and HA-tagged proteins were performed using protein G agarose beads (Roche) and mouse anti-FLAG (Sigma-Aldrich Chemicals) and rat anti-HA (Roche), respectively. The same antibodies were used to detect the respective fusion proteins by western blotting analyses. For ubiquitination assays, EGL-3::HA was immunoprecipitated with anti-HA antibodies, followed by western blot analyses with anti-Myc antibodies (Santa Cruz Biotechnology) to detect Myc-ubiquitin. These blots were stripped and re-probed with an anti-HA antibody to detect EGL-3::HA. Typically, 5% of lysate used in immunoprecipitation experiments was loaded as input controls. Half of the immunoprecipitation reaction was analysed by western analysis, except for Supplementary Figure S9C, where 20% of the immunoprecipitation reaction was analysed for wild-type FSN-1 co-transfection and three times the amount was used for FSN-1(hp2) to aid visualization of weak FSN-1(hp2)::FLAG/EGL-3::HA interaction.

Supplementary data

Supplementary data are available at *The EMBO Journal* Online (http://www.embojournal.org).

Acknowledgements

We thank the *Caenorhabditis Genetics Center* and National Bioresource Project (Japan) for strains, D Durocher, AC Gingras, H McNeill and T Pawson for reagents. This work is supported by Canadian Institute of Health Research MOP93619 to MZ.

Author contribution: WLH designed and performed molecular genetics and biochemistry experiments, and wrote the manuscript. CH performed molecular genetic studies. SBG performed electrophysiology analysis. EHL and JC contributed to genetic analyses. EHL and CS performed the EM analysis. YW and HL helped plasmid and strain construction. MZ designed experiments and wrote the manuscript. EHL, CS and J-LB edited the manuscript.

Conflict of interest

The authors declare that they have no conflict of interest.

References

Abrams B, Grill B, Huang X, Jin Y (2008) Cellular and molecular determinants targeting the *Caenorhabditis elegans* PHR protein RPM-1 to perisynaptic regions. *Dev Dyn* **237:** 630–639

Assadi M, Sharpe JC, Snell C, Loh YP (2004) The C-terminus of prohormone convertase 2 is sufficient and necessary for Raft association and sorting to the regulated secretory pathway. *Biochemistry* **43:** 7798–7807

Berdichevsky A, Viswanathan M, Horvitz HR, Guarente L (2006) *C. elegans* SIR-2.1 interacts with 14-3-3 proteins to activate DAF-16 and extend life span. *Cell* **125:** 1165–1177

Bloom AJ, Miller BR, Sanes JR, DiAntonio A (2007) The requirement for Phr1 in CNS axon tract formation reveals the corticostriatal boundary as a choice point for cortical axons. *Genes Dev* **21:** 2593–2606

Burgess RW, Peterson KA, Johnson MJ, Roix JJ, Welsh IC, O'Brien TP (2004) Evidence for a conserved function in synapse formation reveals Phr1 as a candidate gene for respiratory failure in newborn mice. *Mol Cell Biol* **24:** 1096–1105

Chen Z, Hendricks M, Cornils A, Maier W, Alcedo J, Zhang Y (2012) Two insulin-like peptide antagonistically regulate aversive olfactory learning in *C. elegans*. *Neuron* **77:** 572–585

Chiu SL, Chen CM, Cline HT (2008) Insulin receptor signaling regulates synapse number, dendritic plasticity, and circuit function *in vivo*. *Neuron* **58:** 708–719

Collins CA, Wairkar YP, Johnson SL, DiAntonio A (2006) Highwire restrains synaptic growth by attenuating a MAP kinase signal. *Neuron* **51:** 57–69

Cornils A, Gloeck M, Chen Z, Zhang Y, Alcedo J (2011) Specific insulin-like peptides encode sensory information to regulate distinct developmental processes. *Development* **138:** 1183–1193

De Felice FG, Vieira MN, Bomfim TR, Decker H, Velasco PT, Lambert MP, Viola KL, Zhao WQ, Ferreira ST, Klein WL (2009) Protection of synapses against Alzheimer's-linked toxins: insulin signaling prevents the pathogenic binding of Abeta oligomers. *Proc Natl Acad Sci USA* **106:** 1971–1976

Fiala JC (2005) Reconstruct: a free editor for serial section microscopy. *J Microscopy* **218:** 52–61

Gao S, Zhen M (2011) Action potentials drive body wall muscle contractions in *Caenorhabditis elegans*. *Proc Natl Acad Sci USA* **108:** 2557–2562

Gault VA, Holscher C (2008) Protease-resistant glucose-dependent insulinotropic polypeptide agonists facilitate hippocampal LTP and reverse the impairment of LTP induced by beta-amyloid. *J Neurophysiol* **99:** 1590–1595

Gems D, Sutton AJ, Sunermeyer ML, Albert PS, King KV, Edgley ML, Larsen PL, Riddle DL (1998) Two pleiotropic classes of daf-2 mutation affect larval arrest, adult behavior, reproduction and longevity in *Caenorhabditis elegans*. *Genetics* **150:** 129–155

Golden JW, Riddle DL (1982) A pheromone influences larval development in the nematode *Caenorhabditis elegans*. *Science* **218:** 578–580

Grill B, Bienvenut WV, Brown HM, Ackley BD, Quadroni M, Jin Y (2007) *C. elegans* RPM-1 regulates axon termination and synaptogenesis through the Rab GEF GLO-4 and the Rab GTPase GLO-1. *Neuron* **55:** 587–601

Grill B, Chen L, Tulgren ED, Baker ST, Bienvenut W, Anderson M, Quadroni M, Jin Y, Garner CC (2012) RAE-1, a novel PHR binding protein, is required for axon termination and synapse formation in *Caenorhabditis elegans*. *J Neurosci* **32:** 2628–2636

Hammarlund M, Nix P, Hauth L, Jorgensen EM, Bastiani M (2009) Axon regeneration requires a conserved MAP kinase pathway. *Science* **323:** 802–806

Han S, Witt RM, Santos TM, Polizzano C, Sabatini BL, Ramesh V (2008) Pam (protein associated with Myc) functions as an E3 ubiquitin ligase and regulates TSC/mTOR signaling. *Cell Signal* **20:** 1084–1091

Hao Y, Hu Z, Sieburth D, Kaplan JM (2012) RIC-7 promotes neuropeptide secretion. *PLoS Genet* **8:** e1002464

Hendricks M, Mathuru AS, Wang H, Silander O, Kee MZ, Jesuthasan S (2008) Disruption of Esrom and Ryk identifies the roof plate boundary as an intermediate target for commissure formation. *Mol Cell Neurosci* **37:** 271–283

Hu Z, Pym EC, Babu K, Vashilishan Murray AB, Kaplan JM (2011) A neuropeptide-mediated stretch response links muscle contraction to changes in neurotransmitter release. *Neuron* **71:** 92–102

Hung W, Hwang C, Po MD, Zhen M (2007) Neuronal polarity is regulated by a direct interaction between a scaffolding protein, Neurabin, and a presynaptic SAD-1 kinase in *Caenorhabditis elegans*. *Development* **134:** 237–249

Husson SJ, Clynen E, Baggerman G, De Loof A, Schoofs L (2005) Discovering neuropeptides in *Caenorhabditis elegans* by two dimensional liquid chromatography and mass spectrometry. *Biochem Biophys Res Comm* **335:** 76–86

Husson SJ, Clynen E, Baggerman G, Janssen T, Schoofs L (2006) Defective processing of neuropeptide precursors in *Caenorhabditis elegans* lacking proprotein convertase 2 (KPC-2/EGL-3): mutant analysis by mass spectrometry. *J Neurochem* **98:** 1999–2012

Kaletsky R, Murphy CT (2010) The role of insulin/IGF-like signaling in *C. elegans* longevity and aging. *Disease Models Mech* **3:** 415–419

Kass J, Jacob TC, Kim P, Kaplan JM (2001) The EGL-3 proprotein convertase regulates mechanosensory responses of *Caenorhabditis elegans*. *J Neurosci* **21:** 9265–9272

Kenyon C (2010) The genetics of ageing. *Nature* **464:** 504–512

Kenyon C, Chang J, Gensch E, Rudner A, Tabtiang R (1993) A *C. elegans* mutant that lives twice as long as wild type. *Nature* **366:** 461–464

Kimura KD, Tissenbaum HA, Liu Y, Ruvkun G (1997) daf-2, an insulin receptor-like gene that regulates longevity and diapause in *Caenorhabditis elegans*. *Science* **277:** 942–946

Kleeman GA, Murphy CT (2009) The endocrine regulation of aging in *Caenorhabditis elegans*. *Mol Cell Endocrinol* **299:** 51–57

Klockener T, Hess S, Belgardt BF, Paeger L, Verhagen LA, Husch A, Sohn JW, Hampel B, Dhillon H, Zigman JM, Lowell BB, Williams KW, Elmquist JK, Horvath TL, Kloppenburg P, Bruning JC (2011) High-fat feeding promotes obesity via insulin receptor/PI3K-dependent inhibition of SF-1 VMH neurons. *Nat Neurosci* **14:** 911–918

Kwon ES, Narasimhan SD, Yen K, Tissenbaum HA (2010) A new DAF-16 isoform regulates longevity. *Nature* **466:** 498–502

Landis JN, Murphy CT (2010) Integration of diverse inputs in the regulation of *Caenorhabditis elegans* DAF-16/FOXO. *Dev Dyn* **239:** 1405–1412

Lee HK, Kumar P, Fu Q, Rosen KM, Querfurth HW (2009) The insulin/Akt signaling pathway is targeted by intracellular beta-amyloid. *Mol Biol Cell* **20:** 1533–1544

Lee RY, Hench J, an Ruvkun G (2001) Regulation of *C. elegans* DAF-16 and its human ortholog FKHRL1 by the daf-2 insulin-like sigaling pathway. *Curr Biol* **11:** 1950–1957

Lee SS, Kennedy S, Tolonen AC, Ruvkun G (2003) DAF-16 target genes that control *C. elegans* life-span and metabolism. *Science* **300:** 644–647

Lewcock JW, Genoud N, Lettieri K, Pfaff SL (2007) The ubiquitin ligase Phr1 regulates axon outgrowth through modulation of microtubule dynamics. *Neuron* **56:** 604–620

Li C, Kim K, Nelson LS (1999) FMRFamide-related neuropeptide gene family in *Caenorhabditis elegans*. *Brain Res* **848:** 26–34

Li W, Kennedy SG, Ruvkun G (2003) Daf-28 encodes a *C. elegans* insulin superfamily member that is regulated by environmental cues and acts in the DAF-2 signaling pathway. *Genes Dev* **17:** 844–858

Liao EH, Hung W, Abrams B, Zhen M (2004) An SCF-like ubiquitin ligase complex that controls presynaptic differentiation. *Nature* **430:** 345–350

Liao FF, Xu H (2009) Insulin signaling in sporadic Alzheimer's disease. *Sci Signal* **2:** pe36

Lin CH, Tomioka M, Pereira S, Sellings L, Iino Y, van der Kooy D (2010) Insulin signaling plays a dual role in *Caenorhabditis elegans* memory acquisition and memory retrieval. *J Neurosci* **30:** 8001–8011

Lin K, Hsin H, Libina N, Kenyon C (2001) Regulation of the *Caenorhabditis elegans* longevity protein DAF-16 by insulin/IGF-1 and germline signaling. *Nat Genet* **28:** 139–145

Malide D, Seidah NG, Chretien M, Bendayan M (1995) Electron microscopic immunocytochemical evidence for the involvement

of the convertases PC1 and PC2 in the processing of proinsulin in pancreatic beta-cells. *J Histo Cyto* **43:** 11–19

Man HY, Lin JW, Ju WH, Ahmadian G, Liu L, Becker LE, Sheng M, Wang YT (2000) Regulation of AMPA receptor-mediated synaptic transmission by clathrin-dependent receptor internalization. *Neuron* **25:** 649–662

Mellem JE, Brockie PJ, Madsen DM, Maricq AV (2008) Action potentials contribute to neuronal signaling in *C. elegans*. *Nat Neurosci* **11:** 865–867

Mielke JG, Wang YT (2005) Insulin exerts neuroprotection by counteracting the decrease in cell-surface GABA receptors following oxygen-glucose deprivation in cultured cortical neurons. *J Neurochem* **92:** 103–113

Morris JZ, Tissenbaum HA, Ruvkun G (1996) A phosphatidylinositol-3-OH kinase family member regulating longevity and diapause in *Caenorhabditis elegans*. *Nature* **382:** 536–539

Mukhopadhyay A, Oh SW, Tissenbaum HA (2006) Worming pathway to and from DAF-16/FOXO. *Exp Gerontol* **41:** 928–934

Muller L, Cameron A, Fortenberry Y, Apletalina EV, Lindberg I (2000) Processing and sorting of the prohormone convertase 2 propeptide. *J Biol Chem* **275:** 39213–39222

Murakami H, Bessinger K, Hellmann J, Murakami S (2005) Aging-dependent and -independent modulation of associative learning behavior by insulin/insulin-like growth factor-1 signal in *Caenorhabditis elegans*. *J Neurosci* **25:** 10894–10904

Murphy CT, Lee SJ, Kenyon C (2007) Tissue entrainment by feedback regulation of insulin gene expression in the endoderm of *Caenorhabditis elegans*. *Proc Natl Acad Sci USA* **104:** 19046–19050

Murthy V, Han S, Beauchamp RL, Smith N, Haddad LA, Ito N, Ramesh V (2004) Pam and its ortholog highwire interact with and may negatively regulate the TSC1.TSC2 complex. *J Biol Chem* **279:** 1351–1358

Nakata K, Abrams B, Grill B, Goncharov A, Huang X, Chisholm AD, Jin Y (2005) Regulation of a DLK-1 and p38 MAP kinase pathway by the ubiquitin ligase RPM-1 is required for presynaptic development. *Cell* **120:** 407–420

Ogg S, Paradis S, Gottlieb S, Patterson GI, Lee L, Tissenbaum HA, Ruvkun G (1997) The Fork head transcription factor DAF-16 transduces insulin-like metabolic and longevity signals in *C. elegans*. *Nature* **389:** 994–999

Orci L, Ravazzola M, Storch MJ, Anderson RG, Vassalli JD, Perrelet A (1987) Proteolytic maturation of insulin is a post-Golgi event which occurs in acidifying clathrin-coated secretory vesicles. *Cell* **49:** 865–868

Pan CL, Peng CY, Chen CH, McIntire S (2011) Genetic analysis of age-dependent defects of the *Caenorhabditis elegans* touch receptor neurons. *Proc Natl Acad Sci USA* **108:** 9274–9279

Paradis S, Ailion M, Toker A, Thomas JH, Ruvkun G (1999) A PDK1 homolog is necessary and sufficient to transduce AGE-1 PI3 kinase signals that regulate diapause in *Caenorhabditis elegans*. *Genes Dev* **13:** 1438–1452

Paradis S, Ruvkun G (1998) *Caenorhabditis elegans* Akt/PKB transduces insulin receptor-like signals from AGE-1 PI3 kinase to the DAF-16 transcription factor. *Genes Dev* **12:** 2488–2498

Pierce SB, Costa M, Wisotzkey R, Devadhar S, Homburger SA, Buchman AR, Ferguson KC, Heller J, Platt DM, Pasquinelli AA, Liu LX, Doberstein SK, Ruvkun G (2001) Regulation of DAF-2 receptor signaling by human insulin and ins-1, a member of the unusually large and diverse *C. elegans* insulin gene family. *Genes Dev* **15:** 672–686

Plum L, Belgardt BF, Bruning JC (2006) Central insulin action in energy and glucose homeostasis. *J Clin Invest* **116:** 1761–1766

Po MD, Hwang C, Zhen M (2010) PHRs: bridging axon guidance, outgrowth and synapse development. *Curr Opin Neurobiol* **20:** 100–107

Richmond JE, Jorgensen EM (1999) One GABA and two acetylcholine receptors function at the *C. elegans* neuromuscular junction. *Nat Neurosci* **2:** 791–797

Riddle DL, Swanson MM, Albert PS (1981) Interacting genes in nematode dauer larva formation. *Nature* **290:** 668–671

Rostaing P, Weimer RM, Jorgensen EM, Triller A, Bessereau JL (2004) Preservation of immunoreactivity and fine structure of adult *C. elegans* tissues using high-pressure freezing. *J Histochem Cytochem* **52:** 1–12

Saiga T, Fukuda T, Matsumoto M, Tada H, Okano HJ, Okano H, Nakayama KI (2009) Fbxo45 forms a novel ubiquitin ligase complex and is required for neuronal development. *Mol Cell Biol* **29:** 3529–3543

Stettler H, Suri G, Speiss M (2005) Proprotein convertase PC3 is not a transmembrane protein. *Biochemistry* **44:** 5339–5345

Stigloher C, Zhan H, Zhen M, Richmond J, Bessereau JL (2011) The presynaptic dense projection of the *Caenorhabditis elegans* cholinergic neuromuscular junction localizes synaptic vesicles at the active zone through SYD-2/liprin and UNC-10/RIM-dependent interactions. *J Neurosci* **31:** 4388–4396

Tank EMH, Rodger KE, Kenyon C (2011) Spontaneous age-related neurite branching in *Caenorhabditis elegans*. *J Neurosci* **31:** 9279–9288

Tomioka M, Adachi T, Suzuki H, Kunitomo H, Schafer WR, Iino Y (2006) The insulin/PI 3-kinase pathway regulates salt chemotaxis learning in *Caenorhabditis elegans*. *Neuron* **51:** 613–625

Tong M, Dong M, de la Monte SM (2009) Brain insulin-like growth factor and neurotrophin resistance in Parkinson's disease and dementia with Lewy bodies: potential role of manganese neurotoxicity. *J Alzheimers Dis* **16:** 585–599

Toth ML, Malentijevic I, Shah L, Bhatia A, Lu K, Talwar A, Naji H, Ibanez-Ventoso C, Ghose P, Jevince A, Xue J, Herndon LA, Bhanot G, Rongo C, Hall DH, Driscoll M (2012) Neurite sprouting and synapse deterioration in the aging *Caenorhabditis elegans* nervous system. *J Neurosci* **32:** 8778–8790

Tropea D, Giacometti E, Wilson NR, Beard C, McCurry C, Fu DD, Flannery R, Jaenisch R, Sur M (2009) Partial reversal of Rett Syndrome-like symptoms in MeCP2 mutant mice. *Proc Natl Acad Sci USA* **106:** 2029–2034

Uehara M, Yaoi Y, Suzuki M, Takata K, Tanaka S (2001) Differential localization of prohormone convertases PC1 and PC2 in two distinct types of secretory granules in rat pituitary gonadotrophs. *Cell Tissue Res* **304:** 43–49

Villeneuve P, Lafortune L, Seidah NG, Kitabgi P, Beaudet A (2000) Immunohistochemical evidence for the involvement of protein convertases 5A and 2 in the processing of pro-neurotensin in rat brain. *J Comp Neurol* **424:** 461–475

White JG, Southgate E, Thomson JN, Brenner S (1986) The structure of the nervous system of the nematode *Caenorhabditis elegans*. *Philos Trans R Soc Lond B Biol Sci* **314:** 1–340

Wu C, Daniels RW, DiAntonio A (2007) DFsn collaborates with highwire to down-regulate the Wallenda/DLK kinase and restrain synaptic terminal growth. *Neural Dev* **2:** 16

Zhen M, Huang X, Bamber B, Jin Y (2000) Regulation of presynaptic terminal organization by *C. elegans* RPM-1, a putative guanine nucleotide exchanger with a RING-H2 finger domain. *Neuron* **26:** 331–343

Zhou A, Martin S, Lipkind G, LaMendola J, Steiner DF (1998) Regulatory roles of the P domain of the subtilisin-like prohormone convertases. *J Biol Chem* **273:** 11107–11114

